Hindawi Publishing Corporation
Journal of Nanomaterials
Volume 2008, Article ID 874213, 18 pages
doi:10.1155/2008/874213

Review Article

Toward a Detailed Understanding of Si(111)-7 × 7 Surface and Adsorbed Ge Nanostructures: Fabrications, Structures, and Calculations

Ye-Liang Wang, Hai-Ming Guo, Zhi-Hui Qin, Hai-Feng Ma, and Hong-Jun Gao

Nanoscale Physics & Devices Laboratory, Institute of Physics, Chinese Academy of Sciences, P.O. Box 603, Beijing 100080, China

Correspondence should be addressed to Hong-Jun Gao, hjgao@aphy.iphy.ac.cn

Received 30 August 2007; Accepted 11 January 2008

Recommended by Jun Lou

Firstly, both the rest atoms and the adatoms of Si(111)-7×7 surface are observed simultaneously by scanning tunneling microscopy (STM) when the sample bias voltages are kept less than − 0.7 V. The visibility of the rest atoms is rationalized by first-principle calculations and a very sharper tip can resolve them. Secondly, the behaviors of various Ge nanostructures fabricated on Si(111)-7 × 7, ranging from the initial adsorption sites of individual Ge atoms to the aggregation patterns of Ge nanoclusters, and then to 2D extended Ge islands, are comprehensively investigated by STM. The individual Ge atoms tend to substitute for Si adatoms at Si(111)-7 × 7 with the preference of corner adatoms in the faulted half unit when keeping substrate at 150°C. With increasing Ge coverage, individual Ge atoms and Ge nanoclusters coexist on the substrate. Subsequently, the density of Ge nanoclusters increase and cluster-distribution becomes gradually regular with the formation of final 2D extended hexagonal configuration. When keeping the substrate at 300°C, Ge islands consisting of more complicated reconstructions with intermixing Ge/Si components are present on the substrate. The detail structural characterizations and the bonding nature of the observed Ge nanostructures are enunciated by the first-principle calculations.

1. "ULTIMATE" STM IMAGES OF THE Si(111)-7 × 7 SURFACE

Si(111)-7 × 7 surface as one of the most complicated and fascinating objectof study is being extensively used invarious research fields ranging from surface science and material science to nanotechnology. As a classic example, this reconstructed surface provides a platform for the testing of the unprecedented resolution of STM as a novel powerful apparatus in the early 1980s [1]. The first real space atomic image of this surface was obtained by Binnig et al. in their landmark STM experiment [2], in which twelve bright spots corresponding to the topmost adatoms are revealed.

Since then, with this powerful tool and the later family of scanning probe microscope, the structure of Si(111)-7 × 7 surface has been extensively investigated [3–8]. The demonstrations on the atomic topography of clean Si(111)-7 × 7 surface commonly show the topmost adatoms. On the mapping of rest atoms of Si(111)-7 × 7 surface, some saddle points at the position expected for the rest atoms were reported by Avouris and Wolkow [3] and Nishikawa et al. [4] using STM. Recently, some special techniques were used to obtain the images of Si(111)-7 × 7 surface with atomic scale resolution, such as Lantz et al. [5] using scanning force microscopy and Giessibl et al. [6, 7] using atomic force microscopy. Sutter et al. [8] have mapped selectively the rest atoms at a price of suppressing the adatom spots with a monocrystalline semiconductor tip since its energy gap can suppress the tunneling from the adatoms at certain sample bias. STM is very sensitive to states closest to the sample Fermi Energy (E_F). The state of dangling bonds of the adatoms is about 0.4 eV below E_F and that of rest atoms is about 0.8 eV below E_F [9], so it is difficult to map the rest atoms whose dangling bonds state is far from E_F. Up till now, the adatoms and the rest atoms of Si(111)-7×7 surface are still not clearly distinguished simultaneously by using conventional tungsten tip. This inability has led to the perception that the measured tunneling current for semiconductor materials comes mostly from states near the Fermi level instead of the states further away, due to the

exponential dependence of the tunneling probability on the energy level position [10]. We revisit this surface by using STM. The resultant images simultaneously reveal that not only the 12 adatoms but also the 6 rest atoms per (7 × 7) unit cell of Si(111) surface have high contrast. A careful preparation of the STM tips (reducing the radius of the apex) may bethe key to the success, as our first-principle calculations reveal a geometric hindrance effect of the tip apex for imaging of such complex surfaces.

1.1. Experimental

The experiments were performed by using an ultra-high-vacuum (UHV) STM system with a base pressure of ∼5 × 10^{-11} mbar. The sample was an antimony-doped *n*-type Si(111) wafer (resistance ∼ 0.03 Ω·cm, thickness ∼0.5 mm). Before being introduced into the vacuum chamber, the sample is cleaned by ethanol in an ultrasonic bath and rinsed thoroughly by deionized water. It was degassed at about 600°C in the chamber for several hours. Then, the sample was annealed by direct current heating while keeping the pressure below 10^{-10} mbar. The annealing cycle consisted of flashing the sample to 1200°C for 20 seconds, rapidly lowering the temperature to about 900°C, and then slowly decreasing the temperature at a pace of 1∼2°C/s to room temperature. Nearly perfect (7 × 7) reconstruction was obtained by this method. Sharp STM tips made of a polycrystalline tungsten wire were etched electrochemically in NaOH solution and subsequently cleaned in ethanol and distilled water. Out of many tips used, however, only three had the ability to produce repeatedly the eighteen-spot STM images (Figure 1) while the others produce only the standard twelve-spot images.

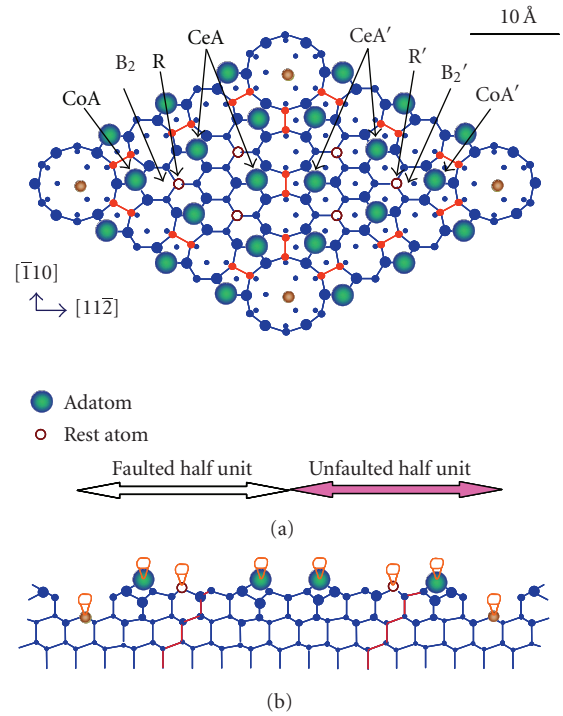

Figure 1: Schematic diagram for Si(111)-7 × 7 "DAS" model [2]. (a) Top view: atoms on (111) layers with the decreasing heights indicated by dots of decreasing sizes. The sites of corner adatom, center adatom, and rest atom in FHUC (labeled CoA, CeA, and R, resp.), and in UHUC (labeled CoA′, CeA′ and R′, resp.), are identified by arrows. Positions B_2 in FHUC, and B_2' in UHUC are also denoted by arrows. (b) Side view: dangling bonds are located at the topmost of all adatoms, rest atoms, and holes.

1.2. Imaging simultaneously the rest atoms and adatoms

The atomic arrangement of the Si(111)-7 × 7 reconstructed surface can be described by a commonly accepted dimer-adatom-stacking (DAS) fault model [11], as schematically shown in Figure 1. This model consists of twelve adatoms and six rest atoms, which are evenly distributed in the faulted half unit cell (FHUC) and unfaulted half unit cell (UHUC). Each unit cell contains nineteen dangling bonds perpendicular to the surface, twelve for the adatoms and six for rest atoms and one for corner atom below the vacancy. The tunneling current in STM of the Si(111)-7 × 7 surface originates from these dangling bonds. A stacking fault exists between the second and third atom layers in the FHUC side (the interlayer bonding rotates 60°), which makes the FHUC more reactive than the UHUC. The large unit cell size (2.7 nm×2.7 nm) makes this surface an ideal template for the growth of well-ordered nanostructures.

Figures 2(a) and 2(b) show STM images with high contrast. They demonstrate simultaneously the adatoms and the rest atoms, that is, 18 topographic maxima per (7 × 7) unit cell. The high-resolution image (Figure 2(b)) presents more clearly all of them. In the UHUC side, the rest atoms appear to have almost the same brightness as the central adatoms, whereas in the FHUC, the rest atoms appear to have considerably less brightness than the central adatoms. The line profile in Figure 2(c) showed the positions and height differences of the six distinct types of atoms (labeled 1 to 6) along the solid line depicted in Figure 2(b). The ranking of height of these atoms is as follows: 1 is the highest, then 3 and 6 follow, with 2, 4, and 5 being the lowest. The rest atom (site 2) in the FHUC side is at the same level as the rest atom (site 5) in the UHUC side, and they are both even at the same level as the central adatom (site 4) in the UHUC half side. The high contrast between rest atoms and adatoms is even better than the previous results obtained by using scanning force microscopies [5–7]. Very recently, Bassi et al. reported the extremely similar topography of this surface at −1.5 V by using Cr tip [12], they claimed that the Cr tip reduced its convolution effects and enhanced its resolving capability. Here, for the first time, all the rest atoms and adatoms of the Si(111)-7 × 7 surface are simultaneously revealed with high contrast by the conventional W tips. The emergence of rest atoms will be further rationalized below by theoretic analysis.

Noting the defect with the missing of one corner adatom (close to the hole at the left-upper corner of the panel) in Figure 2(b), it shows no influence on its adjacent rest atom, which is still visible and stays its normal position without any lateral distortion. So the absence of local adatom does not

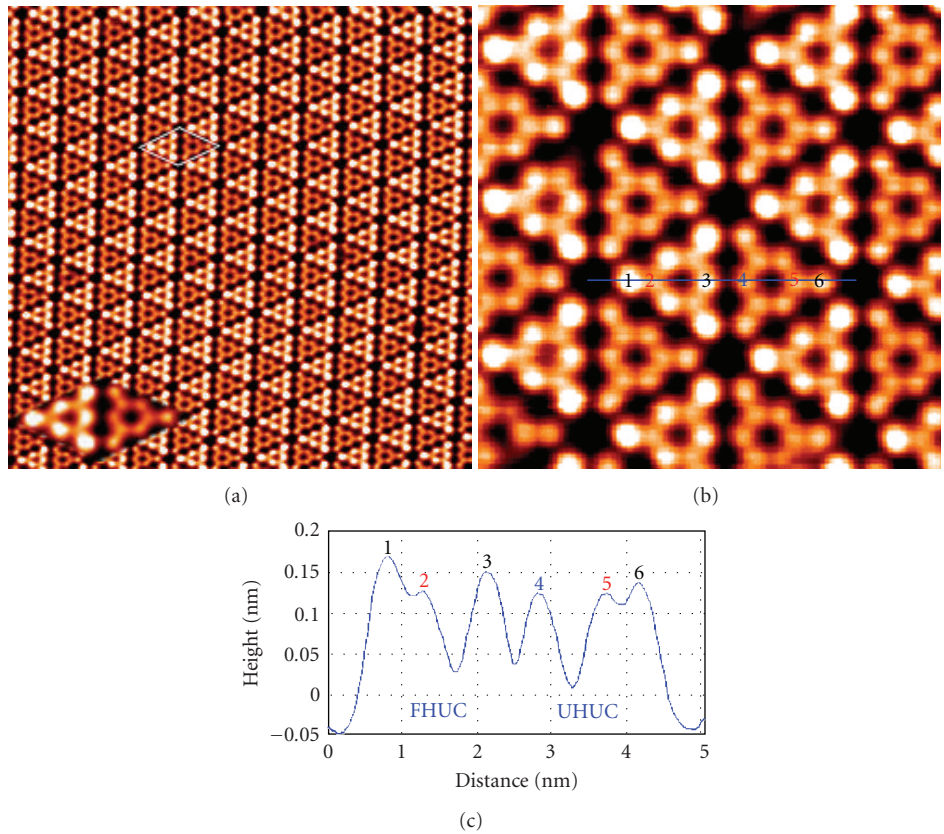

FIGURE 2: Filled-state STM images of Si(111)-7 × 7 surface reveal 12 adatoms and 6 rest atoms per (7 × 7) unit cell. (a) The image extends over an area of 30 nm × 30 nm. The amplificatory (7 × 7) unit cell was indicated in the inset. (b) Amplified image with scanning area of 8 nm × 8 nm. Both images are recorded by sample bias voltage of −1.5 V and tunneling current of 0.3 nA. (c) The line profile taken along the line in (b). Labels "1," "2," and "3" denote the corner adatom, the rest atom, the center adatom in the FHUC, and labels "4", "5", and"6" denote the center adatom, the rest atom, the corner adatom in the UHUC, respectively.

affect the geometric structures of its surrounding atoms in (7 × 7) unit cell. This result coincides with the recent reports about the local structures of adatom vacancies in Si(111)-7 × 7 surface [13]. There, Chen et al. conducted STM dI/dV mappings on adatom vacancies and found that the adatom vacancies showed different local electronic structures but no effect to the geometric or electronic structures of the nearby rest atoms.

1.3. The emergence of rest atoms is dependent on the bias voltage

A sequential STM snapshots obtained at different sample bias voltages, as shown in Figure 3, illustrate that the emergence of rest atoms is dependent on the sample bias voltage. At lower bias voltages of −0.5 and −0.6 V, the images (Figures 3(a) and 3(b)) only show 12 adatoms in each (7 × 7) unit cell. It suggests that the electronic states of adatoms are closer to Fermi level than those of the rest atoms. The absence of the rest atoms ascribes to the electronic states of the rest atoms which are outside the range of the bias when the value of sample bias keeping very low. By further decreasing the value of bias voltage less than −0.7 V, the rest atom spots can be visible, as shown in Figures 3(c)–3(f). It clearly reveals that the dangling bond states of the rest atoms are located at about 0.7 eV below the E_F, which is in excellent agreement with the experimental results measured by the method of current imaging tunneling spectroscopy (CITS). In the year 1989, Hamers et al. measured the electronic banding structure of Si(111)-7 × 7 surface by using CITS. They provided knowledge of the dangling bonds states of the adatoms (about 0.35 eV below the E_F) and the rest atoms (about 0.8 eV below the E_F) [9]. Here, the rest atoms appear to have almost the same brightness as the central adatoms on the UHUC when the bias voltages are less than −0.9 V (see Figures 3(e) and 3(f)).

The STM observations presented here are in sharp contrast to previous STM studies, which in most cases showed images similar to that in Figure 3(a) with 12 protrusions in each (7 × 7) unit, irrespective of the bias voltages (somewhere between −2 V to 2 V). A common explanation for the absence of the rest atom spots in the images relies on the fact that the tunneling probability depends on the thickness of the tunneling barrier [10]. Because the tunneling current is inversely proportional to the exponential of the thickness, the lower-electronic state located in the valence band corresponds to the smaller tunneling current. The rest atoms are invisible but the adatoms are visible may be

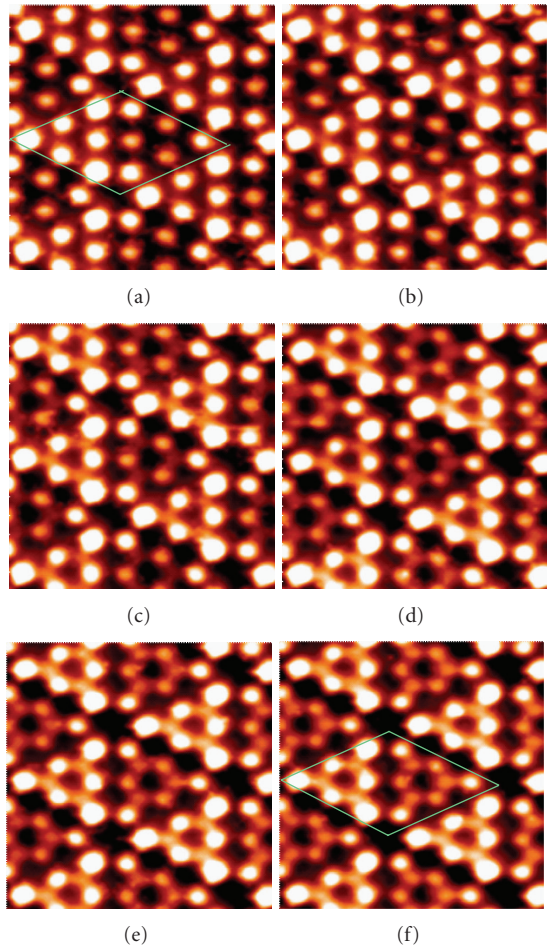

FIGURE 3: STM images of Si(111)-7×7 surface with different sample bias voltages: (a) −0.5, (b) −0.6, (c) −0.7, (d) −0.8, (e) −0.9, (f) −1.0 V, respectively. The rest atoms appear when the sample voltages are less than −0.7 V. All images are taken at tunneling current 0.4 nA in the scanning area of 5 nm × 5 nm.

because the former has significant lower energies than the latter. This argument, however, contradicts the theoretical prediction that the dangling bond states of the rest atoms extended into the vacuum region like the adatoms [14]. Also, because the rest atoms are about 4.6 Å away from the nearest adatoms, if one has an infinitely sharp tip positioned right above the rest atom, there is no reason to believe that the adatoms have effect to screen the rest-atom tunneling. If the tunneling currents from the rest atom were indeed weak, one can move the tip closer to the surface in a constant current STM mode. Thus, this common explanation is probably questionable.

Another possible explanation concerns tip contamination, that is, a few silicon atoms might be accidentally picked up by the tungsten tip during the scan, resulting in a semiconductor tip instead of the original metallic tip. Indeed, recently it has been shown that an InAs semiconductor tip [8] could be used to enhance rest-atom visibility by utilizing the second gap above the fundamental gap (both lie in the Brillouin zone center) of InAs material to suppress tunneling current from the high-lying adatom states. However, a previous study [15] also showed that the local electronic structure of a typical metal/semiconductor interface remains metallic until several monolayers are in the semiconductor. Thus, this is unlikely in the present case with Si atoms adsorption unless the thickness of the contaminant layer exceeds the effective screening length of Si.

1.4. First-principle calculations are in remarkable agreement with experiments

It is impractical for us to experimentally determine what might have happened to the few tips that worked so remarkably well. Instead, we look for a plausible explanation from theory calculations. Our collaborators carried out the calculation by using first-principle density function theory (DFT) [16], as implemented in the VASP codes [17]. The Vanderbilt ultrasoft pseudopotential [18] was used with a cutoff energy equal to 170 eV and one special k-point in the Brillouin zone sum. The surface unit cell contains a slab of six Si layers (without counting the Si adatoms) and a vacuum layer equivalent to six Si layers. The front surface contains the (7×7) reconstruction in the Takayanagi model [11], whereas the back surface is passivated by hydrogen. Except for the bottom layer, all the Si atoms are fully relaxed to minimize the system total energy.

Apparently, the actual tip morphology is complex, possibly with additional atoms adsorbed at the end of the apex, as shown schematically in the inset in Figure 4(f). Because only the lower semispherical part of the tip can be in close proximity with the surface, here the tip is replaced by a sphere of radius r. To further simplify the calculations, only the linescans along the diagonal of the (7×7) unit cell are considered in our simulations.

Figure 4(a) shows the STM image of the Si(111)-7 × 7 surface at a sample bias of −0.57 V. The appearance shows a significant contrast between the FHUC and UHUC of the (7 × 7) unit. At this low sample bias, the electronic states of the rest atoms are outside the range of the bias, as demonstrated in Figures 3(a) and 3(b). Thus, the STM topography here reveals only the twelve topmost adatoms. The adatoms in the FHUC appear noticeably brighter than those in the UHUC. In each half, the adatoms at the corners appear also slightly brighter than those near the center. These qualitative features are in good agreement with the calculated real-space charge distribution at this particular bias (Figure 4(b)). Figure 4(c) shows the STM image at a sample bias −1.5 V. Images of similar quality can be repeatedly reproduced over large area up to 30 nm × 30 nm (Figure 2(a)). We can clearly see both the adatoms and the rest atoms. On the UHUC, they appear to have almost the same brightness as the central adatoms, whereas on the FUHC, the rest atoms appear to have considerably less brightness than the central adatoms. These observations are again in excellent agreement with the calculated real-space charge distribution at the experimental bias in Figure 4(d).

Figure 4(e) shows the calculated linescan at −1.5 V with an infinitely sharp tip, that is, $r = 0$, as has been done

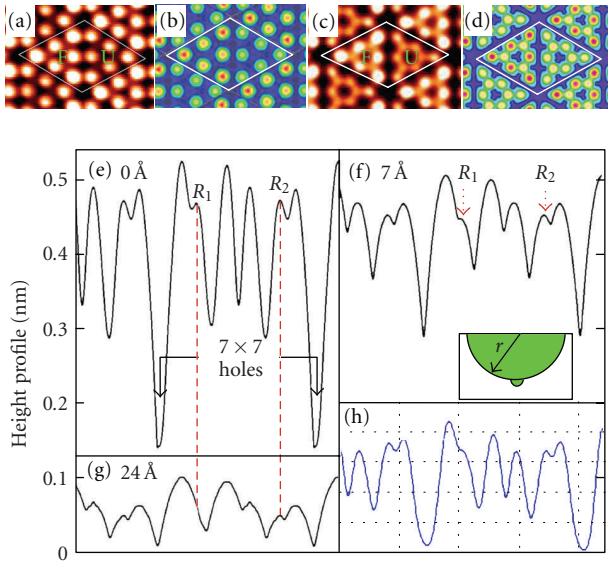

FIGURE 4: (a), (c) Experimental STM images with bias voltage of −0.57 and −1.5 V, and tunneling current of 0.3 and 0.41 nA, respectively. F and U depict the FHUC and UHUC, respectively. (b), (d) Calculated STM images for Si(111)-7 × 7 at − 0.57 and −1.5 V, respectively. The red peaks are about 2 Å above the dark blue borderlines. (e), (f), and (g) are the calculated height profiles along the diagonal of the (7 × 7) unit cell with a tip apex radius r = 0.0, 7.0, and 24.0 Å, respectively. (h) The experimental profile. The inset in (f) schematically shows an STM tip with an adsorbed cluster beneath the apex.

before in most STM image simulations [19]. A sharp tip is also assumed in calculating the images in Figures 4(b) and 4(d). Now, we trace this $r = 0$ curve with a disk of radius r, which is a two-dimensional representation of the three-dimensional sphere, to explore geometric hindrance. It is assumed that at each tip position, tunneling takes place at only one spot on the disk. This is reasonable in most cases because tunneling probability diminishes exponentially with distance. However, there are a few exceptions where the disk is nearly or equally distanced from the $r = 0$ curve, that is, at or near the local symmetry points. For simplicity, however, such a tunneling-current double effect is ignored in our simulation.

Our results show that for small disk radius mimicking adsorbed clusters, the line-scan is essentially the same as in Figure 4(e). Figure 4(f) shows the simulated result for r = 7 Å. At this radius, while none of the main surface topological features have been lost, the overall shape of the linescan has been significantly modified, noticeably the depth of the profile, and the size of the atoms being noticeably larger than those in Figure 4(e). Figure 4(g) shows the simulated result for r = 24 Å. At this radius, the rest atom on the FHUC has completely vanished. Even for the UHUC, the contrast between the rest atom spots and the adatom spots has been greatly reduced. Thus, it is clear that the attainable size of the tip apex is the crucial factor in imaging the true charge distribution on the (7×7) surfaces. Figure 4(h) shows the corresponding linescan determined by our experiment. Despite the simplicity of the model, the calculated result for r = 7 Å in Figure 4(f) is in quantitative agreement with experimental observation. Some of the subtle differences between Figures 4(f) and 4(h) could probably ascribe to the tunneling-current double effect.

It is now understood that STM probes the real-space charge distribution near the E_F in a rather delicate way that may or may not reveal the unperturbed real-space charge distribution of the surfaces. Here, For the Si(111)-7 × 7 surface, we show the calculated and experimental voltage-dependent charge distributions of the Si(111)-7 × 7 surface, which reveal simultaneously both the twelve adatoms and six rest atoms in each (7×7) unit cell [20]. The emergence of rest atom is dependent on the bias voltage and the rest atom spots can be visible at the sample bias voltages less than −0.7 V. The first-principle electronic structure calculations also show a strong dependence of the charge distribution on the bias voltage: twelve spots at −0.57 V for the twelve adatoms (see Figure 4(b)), whereas eighteen spots at −1.5 V for the twelve adatoms plus six rest atoms (see Figure 4(d)). Our results suggest that a geometric hindrance due to the finite size of the tip apex could be the reason for the invisibility of the rest atoms in the past experiments. This finding should invoke significant research interest in the design and fabrication of the STM tip and its applications in exploring more detailed information about surface reconstructions and nanostructures.

2. Ge NANOSTRUCTURES ON Si(111)-7 × 7 SURFACES

Low-dimensional structures can provide interesting physical and chemical properties due to their tiny size and shape. The growth of nanostructures with reduced dimensions has been extensively studied, driven by the intrinsic interest in structures as well as the potential technological applications in quantum devices [21]. Recent studies demonstrated the feasibilities and possibilities of growing self-organized nanostructures on periodic solid surfaces. The Si(111)-7 × 7 surface offers unique template for the self-assembly growth of divers nanostructures because of the large number of distinct bonding sites. Recently, "magic" islands and nanoclusters of semiconductor or metal have been grown on this surface [22–26]. Ordered arrays of two-dimensional nanodots/nanoclusters, including Al, Ga, In, Tl, Si, Ge, Sn, Pb, Na, Cu, Au, Ag, were successfully fabricated [27–51]. These self-organized structures are expected to have a smaller size and stronger confinement potentials compared to the lithographically defined clusters [52].

The adsorption of Germanium on the Si(111)-7 × 7 surface has been extensively studied in recent years [40–51, 53–83], because Ge-based nanostructures have potential applications in microelectronics and optoelectronics. Indeed, Ge/Si system naturally has advantage compatible with Si technology. In addition, being currently incorporated in Si structures, Ge can be used to fabricate strained Si layers with enhanced mobility. Therefore, there are renewed activities in Ge-based nanostructures grown on Si surface in expectation of functional devices with unique electronic and optoelectronic properties [53].

The microscopic understanding of the bonding nature of the adsorbed Ge atoms is an essential issue for the controlled fabrication of desired nanostructures, since the initial adsorption nature may affect the growth behaviors of Ge-based quantum dots and films. In spite of numerous investigations, a unified picture for the bonding structures of Ge atoms on Si(111)-7 × 7 surface has not been established. Meanwhile, the formation and transformation process of various Ge nanostructures during the initial growth stages is far from being well understood. Without doubt, they impede the further control of the growth process of Ge nanostructures.

Here, we provide an STM investigation on various Ge nanostructures on Si(111)-7 × 7 surface with different size and geometry, ranging from individual Ge atoms (adsorption sites) to Ge nanoclusters (evolution and aggregation patterns), and then to 2D extended Ge islands (components and bondings). Especially, we go inside the structural characterizations as well as the transformation process and possible mechanisms of the observed Ge nanostructures in association with first-principle calculations.

The preparation of Si(111)-7×7 surface was conducted as described in the part 1. Then Germanium (99.9999% purity) was deposited onto the as-prepared Si(111)-7 × 7 surface by resistive evaporation. The substrate was kept above room temperature (ranging from 100 to 300°C) to facilitate the formation of ordered structures since at room temperature, Ge atoms do not have enough mobility to span the dimer wall after arriving on the Si(111)-7 × 7 surface [59, 61, 68]. During evaporation, the system pressure was better than 5×10^{-10} mbar. A typical deposition rate of 0.01 ML/min was routinely achieved. One monolayer is defined as the atomic density of the unreconstructed Si(111) surface (1 ML = 7.83×10^{14} atoms/cm^2). Each sample was cooled down to room temperature, and then transferred to STM chamber for measurements. All images were acquired in a constant-current mode with an electrochemically etched tungsten tip.

2.1. Direct STM observations of the adsorption sites of Ge atoms

For the adsorption sites of Ge atoms on Si(111)-7×7 surfaces reported in the literatures, X-ray standing wave (XSW) studies of submonolayer Ge deposited on Si(111)-7 × 7 at 300°C done by Patel et al. in 1985 suggested that Ge atoms might occupy substitutional-like sites on the Si(111) plane [69]. However, the precise Ge sites and the bonding structures were not possible to determine in their studies. Also based on XSW measurements, Dev et al. in 1986 proposed that at low coverages (~ 0.5 ML) Ge atoms would prefer to occupy the ontop sites and to bond directly to the Si adatoms and rest atoms which were just below the adsorbed Ge atoms [70]. Reflection electron microscopy and transmission electron diffraction investigations on Ge/Si(111)-7 × 7 prepared at 640°C by Kajiyama et al. in 1989 found evidence that Ge atoms randomly substituted any Si atoms at the top three layers [71]. Core-level photoemission spectroscopy measurements by Carlisle et al. in 1994 provided indirect observations that there was some preference for Ge to replace the Si adatoms for the annealed Ge/Si(111)-7 × 7 samples [72]. More recent measurements using near-edge X-ray absorption spectroscopy and STM did not provide conclusive descriptions of Ge bonding sites on this surface [56, 73, 74].

Some theoretical calculations have also been reported on Ge bonding sites on the Si(111)-7 × 7 surface, however, the calculations provided limited information and showed contradictory results. Early work was semiempirical X_α and extended Hückel calculations with limited predictive capabilities, which provided support for the notion that Ge atoms bond directly to rest atoms or Si adatoms [75–77]. In contrast to the semiempirical calculations, on the other hand, using first-principle density functional calculations, Cho and Kaxiras in 1998 reported a limited exploration of bonding possibilities and found that the most stable adsorption position for Ge on Si(111) is the high-coordination bridge B_2 site (see Figure 1 for pertinent terminology of the Si(111)-7 × 7 surface), which was a bonding site that had not been proposed on the basis of experimental data [78]. They introduced the so-called basins of attraction, which contain stable adsorbate positions as high-coordination sites rather than surface dangling bond sites. Their calculations showed that the rest atoms or intrinsic Si adatoms sites (dangling bond T_1 sites) of substrate were the high-energy sites, and the low-energy sites were the B_2-type sites for Si and Ge adsorption.

Here, we report STM observations and first-principle calculations for the structure of the Ge-adsorbed Si(111)-7 × 7 surface at low Ge coverages. Figure 5 shows STM image of the Si(111)-7 × 7 surface with Ge coverages of 0.02, 0.08, and 0.10 ML, respectively. These images show that the surface lattice retains the original (7 × 7) reconstruction with the dimers and the adatoms. The FHUC and the UHUC of the (7 × 7) reconstruction are distinguished due to the different contrast. The deposited Ge atoms appear as bright protrusions. Three significant features are presented in the STM images. First, the deposited Ge atoms are clearly resolved as individual atoms on the surface. Second, the adsorbed Ge atoms reside on the sites that were occupied by the Si adatoms on Si(111)-7 × 7. Finally, more Ge atoms occupy the corner Si adatom sites in the FHUC than the other Si adatom sites. No Ge atoms are found at either the rest atom or the high-coordination surface sites. Furthermore, profile lines through the bright dots show that the height difference between the Ge atoms and the original Si adatoms is about 0.2 Å in the STM images. This data clearly show that the Si adatom does not stay in its original position (on a clean Si(111)-7 × 7 surface, the Si adatom occupies a so-called T_4 site just above a second-layer Si atom) [11, 79, 80]. As the bond length of Si-Ge is about 2.36 Å, the increased height due to addition of one Ge atom should be reflected in the STM image.

Therefore, the addition mechanism of Ge atop Si adatom is supposed as a questionable explanation. Moreover, the number of dangling bonds will increase to three if a Ge atom adds on the top of one Si adatom, and it is not considered having a suitable total energy. The topographic height undulations of adatom sites in STM images caused by Ge-Si exchange on Si(111)-5 × 5-Ge reconstructions

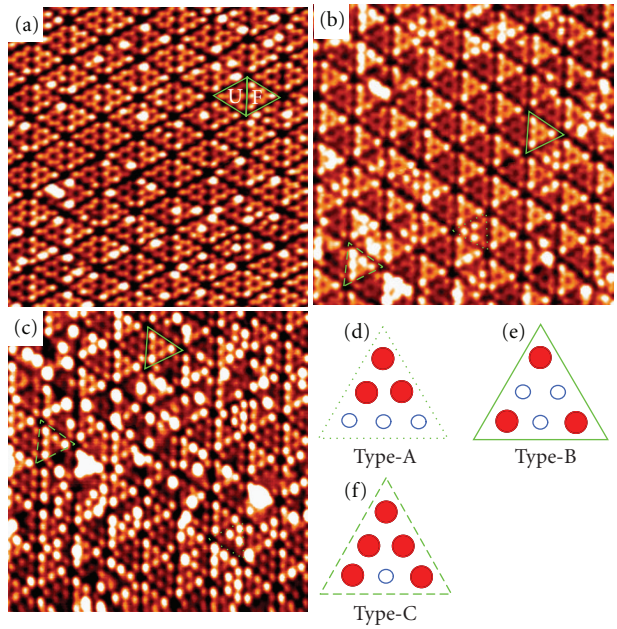

Figure 5: Filled-state STM images (20 nm × 20 nm) of the Si(111)-7 × 7 surface with Ge coverages of (a) 0.02 ML; (b) 0.08 ML; and (c) 0.10 ML. Sample bias: −2.2 V in (a), and −1.5 V in (b) and (c); tunneling current: 0.5 nA in (a), and 0.2 nA in (b) and (c). Three different configurations of Ge protrusion distributions are denoted in (b) and (c) by solid-line triangle, dotted-line triangle, and dashed-line triangle, respectively. The schematics for the three typical Ge patterns, named type-A, type-B, and type-C, are shown in (d), (e), and (f), respectively.

have been proposed by Becker et al. [81] and Fukuda [82], and were also investigated by Rosei et al. [83] with current imaging tunneling spectroscopy. The feature of Ge-Si exchange is confirmed by our recent results, which will be introduced in the following section. Here, we suggest that Ge-Si exchange can also occur during the initial adsorption stage of Ge/Si epitaxy growth due to the structures similarity of Ge and Si. We thus conclude that Ge would prefer to substitute the Si adatoms in its initial adsorption stages.

As shown in Figures 5(b) and 5(c), there are three types of Ge protrusions patterns on the Si(111)-7 × 7 surface. The schematics of these three types patterns, named as type-A, type-B, type-C, are given in Figures 5(d), 5(e), and 5(f), respectively. Type-A illustrates three Ge atoms (red spheres) locating at one corner adatom site and two adjacent center adatom sites in a HUC. Type-B indicates the configuration with three Ge atoms occupying corner adatom sites in a HUC. Type-C refers to the adsorption structure with five Ge atoms residing on the sites of three corner adatoms and two center adatoms in a HUC. Type-B and Type-C distribute preferentially in the FHUCs, as shown in Figures 5(b) and 5(c).

The sites distribution of the bright protrusions at the corner and center adatom sites in both the FHUCs and the UHUCs is illustrated in Figure 6. At the Ge coverage of 0.02 ML, the site preference ratio is about 5.6 : 4.4 for the FHUC to the UHUC, and 6.1 : 3.9 for the corner to the center adatom sites, respectively. When the Ge coverage increases to 0.08 ML, the site preference ratios are about 9 : 1 for the FHUC to the UHUC, and 4 : 1 for the corner to the center adatom sites. The site distribution for the coverage of

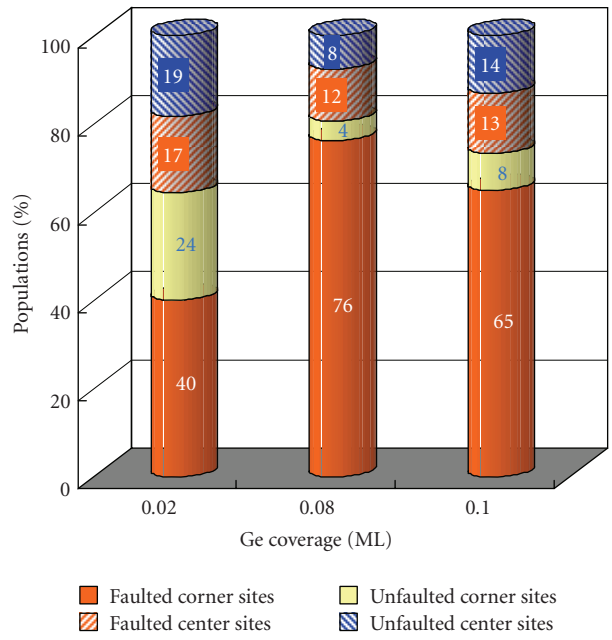

Figure 6: Site distributions of Ge at various adatom positions at coverages of 0.02 ML, 0.08 ML, and 0.10 ML.

0.10 ML is similar to that for the coverage of 0.08 ML. The overall conclusion is that after an initial random occupation of Si adatom sites, corner adatom sites in the FHUC are preferred and gradually type-B patterns become dominant. Type-A and Type-C patterns are more discernible at slightly higher coverages, and finally, small islands begin to appear.

Our collaborators performed first-principle DFT calculations using the pseudopotential method and a plane-wave basis set [16, 17]. The Si(111) surface was modeled by repeated slabs with 4 layers of Si atoms (each layer contained 16 Si atoms, corresponding to a 4×4 surface unit cell) and 4 Si adatoms, separated by a vacuum region of 12 Å. Two of the four rest atoms were saturated by hydrogen, so that the ratio of the number of the adatoms to that of the rest atoms is the same as for the 7×7 surface. Except for the Si atoms in the bottom layer, which were fixed and saturated by H atoms, all the atoms were relaxed until the forces on them were less than 0.05 eV/Å. The exchange-correlation effects were treated with the generalized gradient-corrected exchange-correlation functions given by Perdew and Wang [84]. The Vanderbilt ultrasoft pseudopotentials are adopted [18]. A plane-wave energy cutoff of 14.7 Ry and the point for reciprocal space sampling were used for all the calculations.

All the possible configurations with a Ge atom near an adatom or/and a rest atom were calculated. Two lowest energy configurations, as shown in Figure 7, were found to have essentially the same total energy (the difference in total energy is smaller than 0.02 eV). The first one consists of Ge at a B_2 site (Figure 7(a)), as identified earlier by Cho and Kaxiras [85]. In the second configuration (Figure 7(b)), the adsorbed Ge atom substitutes for an Si adatom and the substituted Si adatom occupies a nearby B_2 site. We refer to the Ge position in the second configuration as S_4 (substitutional site with four nearest-neighboring silicon atoms). The total energies of the configurations with Ge bonded at the ontop positions of adatoms and rest atoms are significantly higher (2.3 and 1.6 eV, resp.) than the B_2 and S_4 configurations. So we can clearly rule out the possibility of such configurations, which were suggested previously on the basis of semiempirical calculations [70, 75, 76].

For both lowest energy configurations (B_2 and S_4), the atom (Si or Ge) at a bridge site may diffuse within a basin (to occupy any of the six B_2 sites near the rest atom) and across basins (to occupy the B_2 sites near different rest atoms). The diffusion barriers within a basin and across basins are about 0.5 eV (0.6 eV) and 1.0 eV (1.0 eV) for the Ge (Si) atoms, respectively, which is in agreement with previous first-principle calculations [77, 86]. Therefore, Ge atoms in the S_4 configurations are thermodynamically more stable than in the B_2 configurations. In particular, after the atoms initially bonded at the B_2 sites migrate to step edges and/or to form islands, the surface exhibits a stable Ge-S_4 configuration, in which Ge atoms substitute for some of the Si adatoms and no atoms are bonded at any of the B_2 sites (Figure 7(c)), as shown by our STM observations. The Ge-S_4 configuration is coincided with the recent results reported by two research groups [46, 61]. They prepared the sample with the same experimental conditions as the current work. In their STM measurements, they also confirmed that Ge replaced Si adatoms on the Si(111)-7×7.

It is well known that the backbonds of the Si adatoms of the Si(111)-7×7 surface are under considerable strain [11, 79, 86]. We therefore suggest that the adsorbed Ge atoms are able to break the backbonds and further replace the Si adatoms at elevated temperatures. Previous studies have established that the corner adatoms in the FHUCs are under more strain than the other adatoms, which implies that backbonds of the corner adatoms in the FHUCs are broken easier than those of the other adatoms [85, 86]. When Ge atoms are deposited on the surface, the chance for the Ge atoms occupying the B_2 sites near a center adatom is larger than that near a corner adatom (the center adatom has two nearby rest atoms while the corner adatom has only one). Thus, the Ge–S_4 bonding structure tends to be preferentially formed at the corner adatom sites and in the FHUCs of the Si(111)-7×7 surface [87].

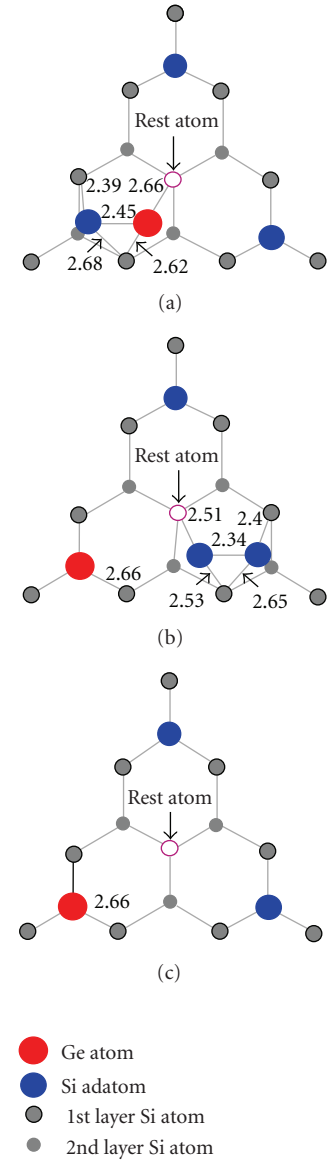

Figure 7: Schematic top view of the calculated lowest energy configurations of a Ge atom on the Si(111) surface: (a) Ge at a B_2 site and the nearby Si adatom at the position of its original site. (b) Ge at the substitutional S_4 site and the Si adatom at a B_2 site. (c) Ge atoms substitute for some of the Si adatoms and no atoms are bonded at any of the B_2 sites. The bond lengths are shown with unit of Å.

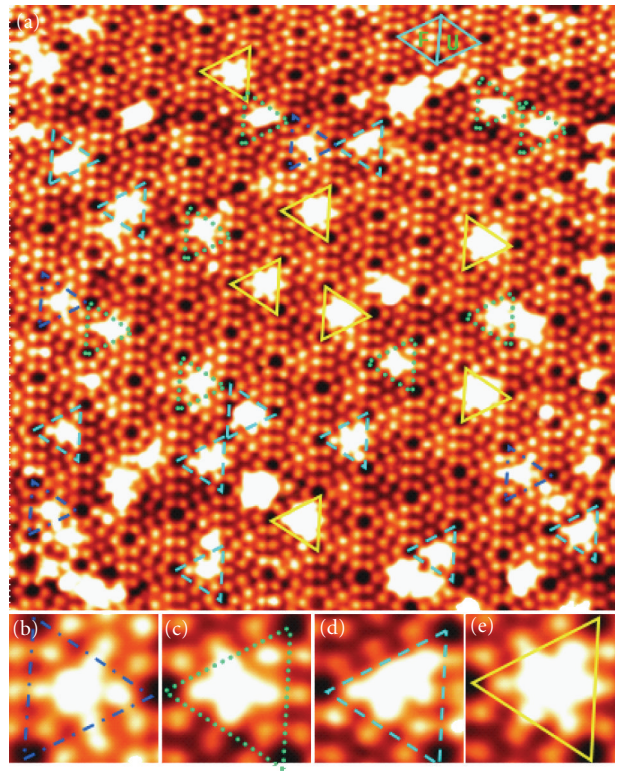

Figure 8: (a) Empty-state STM image (U_b = 2.0 V, I_t = 0.3 nA, 30 nm × 30 nm) of the Si(111)-7 × 7 surface with Ge coverage ~ 0.12 ML. The substrate temperature is held at ~100°C for the Ge deposition. Ge clusters with four typical geometrical configurations, named as type-Tr (triangle), type-Te (tetragonal), type-P (pentagonal), and type-H (hexagonal), are denoted by the triangles with the dotted dash-line, dotted-line, dashed-line, and solid-line, and their magnified images (3 nm × 3 nm) are shown in (b), (c), (d), and (e), respectively.

Finally, the relaxed Ge–S_4 configuration obtained from our calculations shows that the Ge atom resides at the position higher by 0.24 Å than the original Si adatom that has been replaced by Ge, which is in good agreement with our STM data.

2.2. Formation and transformation of Ge clusters

It is of course interesting to study the possible configurations of Ge nanostructures in subsequent Ge depositions. Indeed, with increasing Ge coverage, some novel structures, like small Ge clusters with varying geometrical configurations appear on the Si(111)-7 × 7 surface. The representative image is shown in Figure 8(a) with Ge coverage about 0.12 ML deposited at the substrate temperature ~ 100°C. A remarkable feature in the image is the emergence of Ge clusters with special configurations. Dimer rows and corner-holes of the surface are left uncovered, indicating a strong preference of the Ge clusters to locate in (7 × 7) unit cell. Deposited Ge clusters are imaged as bright bumps and four typical bump structures are distinguished, as named type-Tr, type-Te, type-P, and type-H. Figures 8(b)–8(e) show their magnified images.

Type-Tr (triangle-star-like) cluster emerges like a bright triangle star in a HUC, in this structure three center adatoms and their adjacent high-coordination sites are covered by Ge atoms. Similarly, in the type-Te (tetragonal-star-like), type-P (pentagonal-star-like), and type-H (hexagonal-star-like) clusters, Ge atoms occupy an increasing area in a HUC: type-Te covers one more rest-atom region, type-P covers another one, and type-P covers all three rest-atoms regions.

Four kinds of Ge cluster configurations appear in the same image, it suggests a formation process of Ge clusters from triangle to tetragonal, then to pentagonal, and at last to mature hexagonal-star-like structure despite the fact that we do not observe the real-time evolution of single Ge cluster from simple to complex. Each kind of Ge cluster is observed both in the FHUCs and UHUCs, as shown in Figure 8(a), and there is no clear preference for locating positions of Ge clusters in the FHUCs and UHUCs (37 clusters in the FHUCs and 34 clusters in the UHUCs).

Although the Ge cluster structures on the Si(111)-7 × 7 surface represent the majority in Figure 8(a), while lots of individual Ge atoms locating on the Si adatoms still can be resolved with bright spots at the positions of some Si adatoms in the empty-state STM image. As we know, the STM empty-state images are taken at positive sample bias voltage, corresponding to tunneling electrons from the occupied state of tip to sample. On clean Si(111)-7 × 7 surface, each adatom has a dangling bond and has the same probability to accept the tunneling electrons from tip, so all the adatoms on clean Si(111)-7 × 7 surface have the same brightness in STM empty-state images. By this rule, we can affirm that the brighter protrusions at the sites of Si

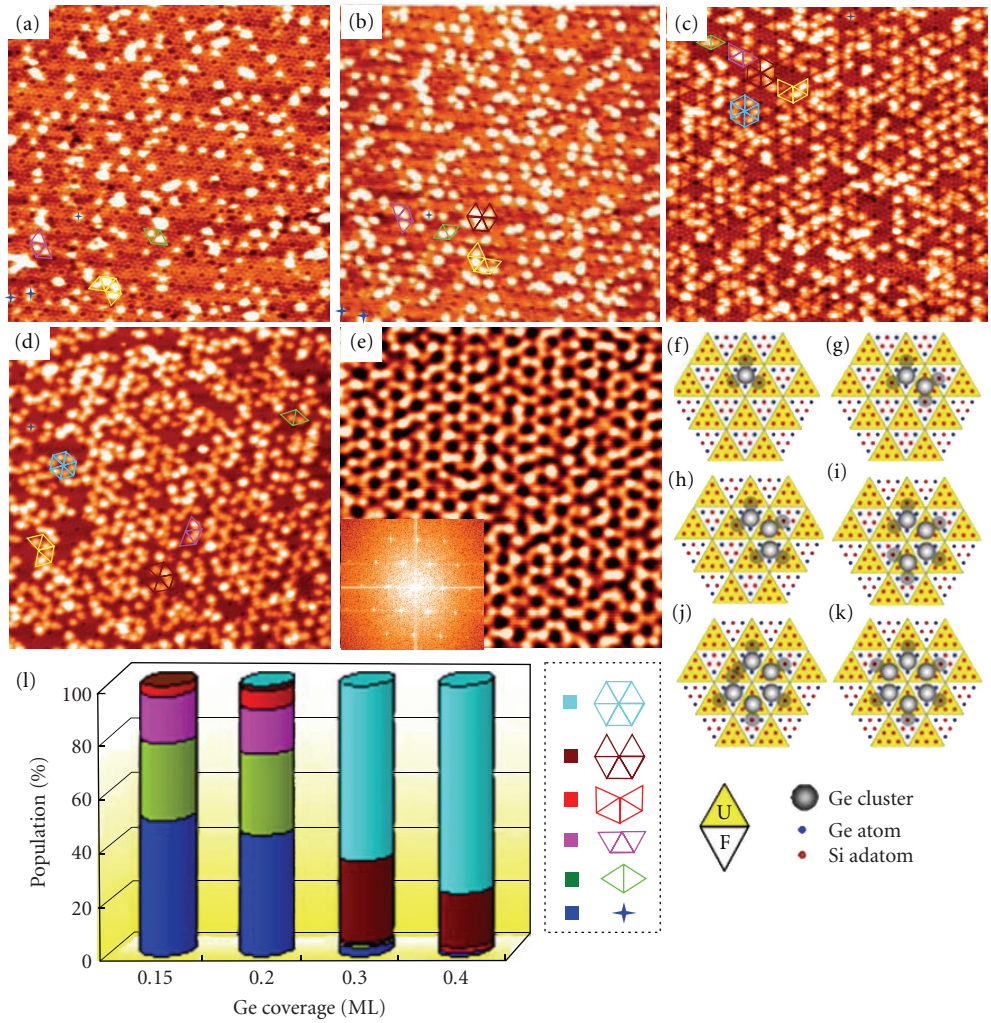

Figure 9: (a)–(e) Series of STM images of Ge-deposited Si(111)-7 × 7 surface show the formation process of hexagonal superlattice with increasing Ge coverages ranging from 0.15, 0.2, 0.3, 0.4 to 0.5 ML, respectively. The substrate temperature is held at ~150°C for Ge deposition. All image sizes are 50 nm × 50 nm. The inset in (e) shows a Fourier transform of the hexagonal arrays. (f)–(k) Schematics illustrating the evolution of cluster structures from open to close hexagonal ring. The Si-center adatoms that transfer charge are shaded in gray. (l) Histograms for the distributions of different local Ge nanostructures at varying coverages. Six distinct local nanostructures are depicted by symbols with different shapes and colors in the STM images.

adatoms are Ge atoms. Thus, individual Ge atoms and some Ge clusters coexist on the Si(111)-7 × 7 surface at proper substrate temperature and Ge coverage.

2.3. *Evolution of hexagonal Ge cluster superlattice*

The above results showed that most Ge atoms form correlated patterns at very low Ge coverages less than 0.1 ML, by replacing the Si adatoms of the Si(111)-7 × 7. With the further increasing of Ge coverage, deposited Ge atoms are constrained inside the HUC and aggregate into the form of clusters with different geometry and atom numbers. In addition, previous results reported the existence of hexagonal Ge nanostructures on Si(111)-7 × 7 [57, 60], however, the detail process and driving force are still not clear. Here, we will further reveal the evolution of hexagonal Ge clusters with increasing Ge coverages. The driving mechanism and the atomic geometry of Ge clusters will be enunciated by STM observations and first-principle calculations.

In Figures 9(a)–9(e), a sequence of STM images at varying Ge coverages show the continuing evolution of the Ge clusters from isolated ones into hexagonal patterns. The appearance illustrates that the density of Ge clusters gradually increases with the increasing Ge coverages. The cluster distribution becomes much regular from disordered arrangement to high-symmetric hexagonal superlattice. Six distinct local cluster patterns can be distinguished in STM images, as marked by different symbols. The schematics in Figures 9(f)–9(k) simply depict the structures of these local cluster patterns, ranging from single Ge clusters, to pair of clusters, to open cluster ring, and finally a close cluster ring with six clusters surrounding a hole in Si(111)-7 × 7 surface. The histograms in Figure 9(l) reveal the distribution feature of six different local Ge nanostructures at varying

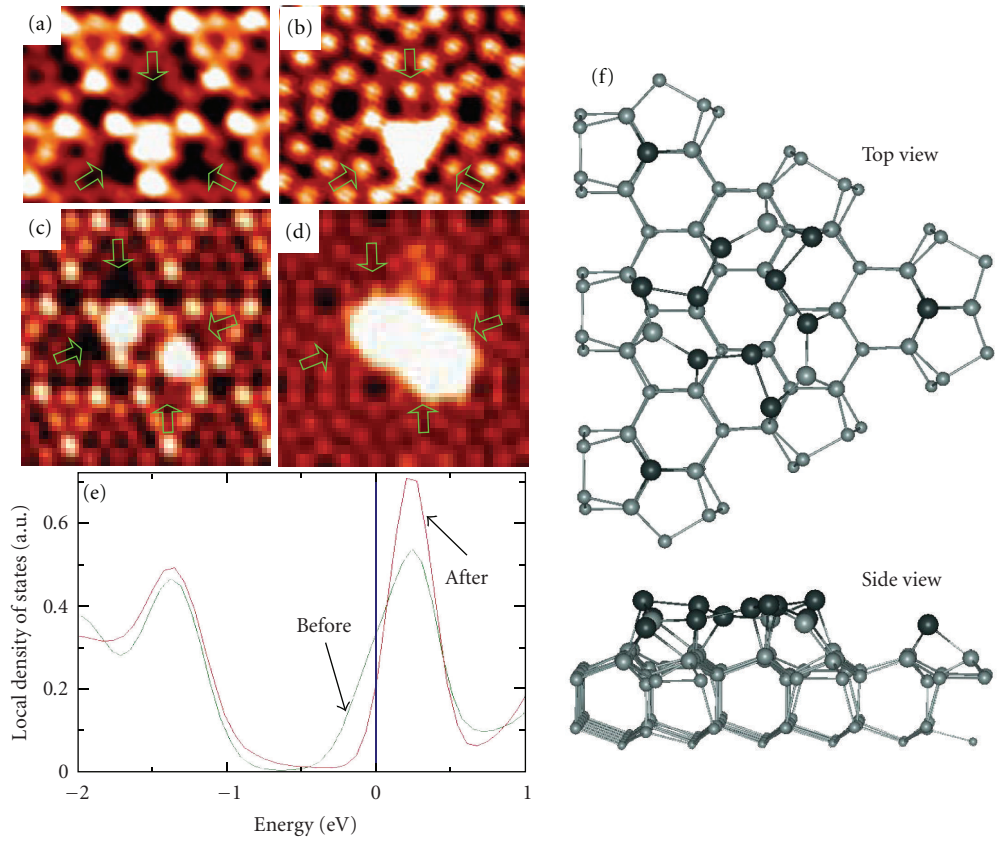

FIGURE 10: Local STM images show the different appearance of Ge-deposited Si(111)-7 × 7 surface with filled-state images (−2.5 V) in (a) and (c) and empty-state image (+2.5 V) in (b) and (d). Single Ge cluster presents in (a) and (b) and double clusters in (c) and (d). The centers Si adatoms, as indicated by the arrows, are invisible in (a) and (c) but visible in (b) and (d). (e) Local density of states projected onto a center Si adatom in a UHUC before and after Ge deposition. The Fermi level is at 0 eV. (f) The corresponding relaxed minimum energy configuration (only the FHUC is shown). The Si and Ge atoms are depicted by gray and dark spheres, respectively. Spheres of decreasing size represent the Si atoms with increasing distances from the surface. The dotted lines show weak bonds.

coverages. The evident tendency is that the ratio of simple cluster pattern reduces with the increase of complex ones.

The distribution tendency suggests the evolution of hierarchical cluster patterns from dispersing clusters to close cluster rings. Most of clusters discretely emerge on the substrate at low coverage of 0.10 ∼ 0.15 ML with an initial preference in the FHUCs (see Figure 9(a)). And then open cluster rings containing three, four, and five clusters, nucleated on the Si(111)-7 × 7 surface at a Ge coverage of ∼ 0.2 ML (Figure 9(b)). Afterwards closed Ge hexagonal rings consisting of six clusters begin to form at a Ge coverage of ∼ 0.3 ML (Figure 9(c)). When the Ge coverage approaches to 0.4 ML, most of the HUCs of both FHUC and UHUC are occupied by Ge clusters. The underlying (7 × 7) surface periodicity and the hexagonal superstructures coexist. Finally, the high-regular hexagonal superlattice forms at a Ge coverage of ∼0.5 ML and covers the entire (7 × 7) surface (Figure 9(e)). The driving mechanism for the cluster evolution, ascribing to the charge transfer from Si center adatoms to Ge clusters, will be further discussed as following in association with DFT calculations.

In Figures 10(a) and 10(b), we show contrasted filled-state STM image at sample bias −2.5 V, and empty-state image at +2.5 V, respectively. The Ge clusters look more compact in the former than in the latter, and they show strong brightness in the center region of the FHUC. An obvious feature is that Ge cluster has a strong effect on its three neighboring UHUCs. The closest Si-center adatoms in the nearest-neighbor UHUCs are invisible in the filled-state image. However, these Si adatoms do exist at their original places in the (7 × 7) reconstruction, as shown by the empty-state image. This fact suggests that the Si-center adatoms in the nearest-neighbor UHUCs transfer charge to the Ge clusters.

As we known, the tunneling electrons transfer from sample to tip for the filled-state imaging, in reverse, they transfer from tip to sample for the empty-state imaging. Here in our measurements, in the filled-state images, the darkened areas (center adatoms) surround the clusters. One reason is due to geometric defect, that is, no adatoms exist at these positions. But the empty-state images prove the existence of the adatoms at the original positions. So, the only reason is that the charge of center adatoms transfers to nearby Ge clusters and resulting in the absence of tunneling electrons from center adatoms in the filled-state images. Thus, the STM measurements demonstrate lateral charge redistributions in Ge-Si system.

The charge transferring from center adatoms to Ge cluster is further revealed by first-principle DFT calculations. For all the minimum-energy configurations, Ge clusters contain 6 ∼ 12 Ge atoms in the FHUC of a (7 × 7) unit cell, and the dangling bond state of the center Si adatoms nearby the FHUC is almost empty, indicating charge transfer of neighboring Si adatoms. Figure 10(e) shows the projected electronic density of states (local density of states, DOS) onto the center Si adatom in an adjacent UHUC before and after the formation of a nine-Ge cluster in an FHUC, see the minimum-energy configuration in Figure 10(f). For clean Si(111)-7 × 7 surface before Ge deposition, the dangling bond state of the center Si adatom is partially occupied and crosses the Fermi level [80, 88, 89]. After the formation of Ge clusters, the occupation of the dangling-bond state is reduced significantly, confirming a charge transfer from the central Si adatom. Such a charge transfer occurs because it can lower the total energy of the system. Self-assembled clusters of various metals formed on Si(111)-7 × 7, which have similar network as Ge clusters, have been reported [24, 27, 28, 90–92]. Several groups suggested that the interaction between the substrate and the metal clusters might play a role for the self-organization [24, 27, 28], and other researchers had emphasized the interaction between the clusters themselves [93]. Charge transfer and its role have not been reported before.

When local coverage is higher, a second Ge clusters may form at the center of an UHUC adjacent to an FHUC already containing a Ge cluster, as shown in Figures 10(c) and 10(d). Similar to the first one, the second Ge cluster darkens the center Si atoms in the two neighboring FHUCs in the filled-state image (Figure 10(c)), which again indicate charge transfer, though the charge transfer is not as effective as in the UHUC. Charge transfer helps us understand the formation of a cluster in an UHUC nearby an existing particle in a FHUC, and further explain the evolution of Ge cluster patterns from isolated one to closed hexagonal patterns [94].

The above results show that a new cluster forms adjacent to an existing FHUC cluster in a neighboring UHUC, and electron transfer occurs from the two new surrounding FHUCs. The two clusters remain distinct with a "dimer wall" separating them as shown in Figure 9(h). First-principle calculations confirm the depletion of charge associating with the dangling bonds of center Si adatoms in the three UHUCs surrounding a Ge cluster in an FHUC, and also a decrease in electronic energy by such a charge transfer. The energy gain can be attributed to "local Madelung energy", which is used in determining the energy of a single ion in a crystal.

Assuming that the amount of charge transferring from any of the center Si adatom is the same q_0, then a single cluster has a central charge of $-3q_0$ (Figure 9(f)). The total energy is lowered by a local Madelung energy of the cluster, that is roughly $(-9/d_1 + 3/d_2)q_0^2$, where d_1 (∼11 Å) is the distance between the Ge clusters and an adjacent Si adatom that has been depleted of charge, and d_2 (∼19 Å) is the distance between two such Si adatoms. Because d_1 is smaller than d_2, the local Madelung energy is negative ($-0.66q_0^2$). When a second cluster forms in an adjacent UHUC, as in Figure 9(h), the charge on each cluster is reduced from $-3q_0$ to $-2q_0$ and the local Madelung energy is approximately $(-8/d_1 + 2/d_2 + 4/d_3)q_0^2 \approx -0.36q_0^2$, where d_3 (∼15.5 Å) is the distance between the two Ge clusters. The local Madelung energy in the Ge cluster pair is smaller than that of single cluster. The reduction in the Madelung energy is used to overcome the factors that inhibit the formation of isolated clusters in UHUCs, and the residual Madelung energy stabilizes the cluster pair. The energy is substantial, and from the DOS curves of Figure 10(e), we estimate $q_0 \approx (0.3–0.5)$ e, whereby the Madelung energy stabilizing a pair is ∼ 0.5–1.3 eV. With the emergence of new Ge clusters, the net charge on each Ge cluster decreases gradually from $3q_0$ in the case of an isolated cluster to $2q_0$, $5/3q_0$, $3/2q_0$, $7/5q_0$, and finally $1q_0$ if a complete isolated hexagon is formed as in the schematic of Figures 9(f)–9(k), and the effective Madelung energy per cluster also gradually reduces. So the reduction of the local Madelung energies contributes to the stabilization of the local cluster structures. Thus here we quantitatively revealed how the charge transfer sustains the evolution of cluster patterns from isolated ones to ordered hexagonal arrays.

2.4. Formation of Ge islands and Ge-Si intermixing at high temperature

The further increase of the substrate temperature causes the coarsening of clusters and intermixing between Ge and Si atoms, which is believed to be due to the enhancing mobility of Ge atoms [43, 44]. When the substrate temperature is increased to about 300°C or even higher temperature, the Ge islands begin epitaxial growth. Deposition of Ge atoms on Si(111)-7 × 7 at room temperatures following by annealing treatment also results in 2D extended Ge islands. Figure 11(a) shows a typical surface morphology of a Ge island with submonolayer Ge coverage. There are three distinct features in this image. First, the reconstruction of the island is (7 × 7), same as the configuration of original substrate, see the close-up STM image in Figure 11(c). Second, the dimer directions of the Ge island are same as that of the substrate which, revealing the supercell of Ge island, has the same alignment as the substrate. Third, the shape of Ge islands is usually close to triangle, similar to the shape of HUC triangle of the substrate. All these features reveal the modulation effect of the substrate to the epitaxy growth of Ge islands.

During the growth of an island, the substrate (7 × 7) reconstruction has to be removed and the surface Si atoms will rearrange to the bulk (1 × 1) structure [95]. It needs to overcome different energy barriers for the removal of the reconstruction in the UHUCs and in the FHUCs [96]. In the UHUC triangles, only the atoms in the topmost layer rearrange, which is associated with a relatively low-energy barrier. However, in the FHUC triangles, the removal of the stacking faults (see the schematic in Figure 1) in the deeper layer below the adatoms is associated with a larger energy barrier. The activation barrier for Ge overgrowth in the FHUCs is clearly higher than in the UHUCs. Thus, the edges of Ge island are comprised of UHUC triangles and surrounded by FHUC triangles of the substrate, as shown in Figures 11(c) and 11(d).

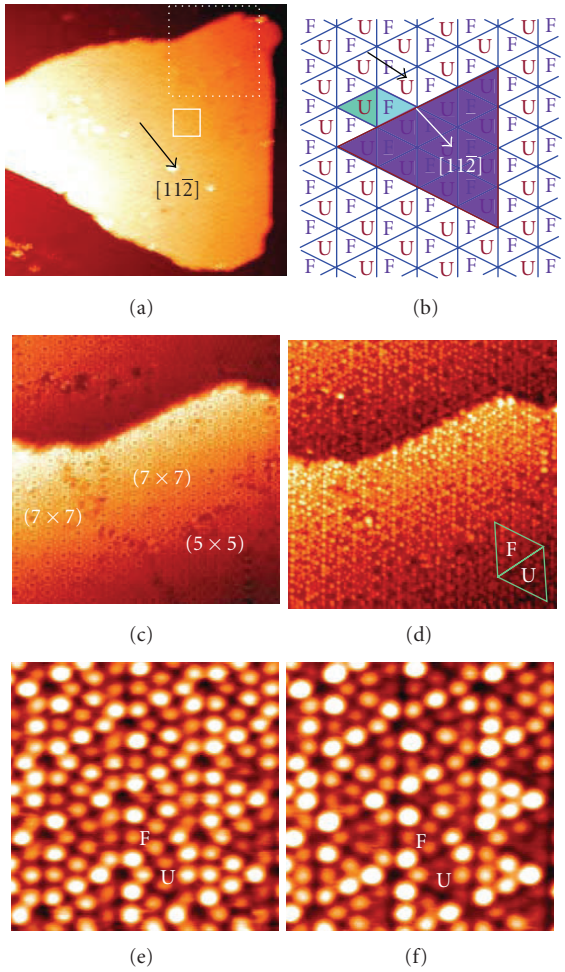

FIGURE 11: (a) STM image shows a typical Ge island on the Si(111)-7 × 7 surface. The substrate temperature was kept at 300°C for Ge deposition. (b) The schematic drawing of the Ge island on (7 × 7) reconstruction. (c) and (d) are amplified images of the area in (a) depicted with a dotted-line square. (7 × 7) and (5 × 5) reconstructions coexist in the island. (e) and (f) are the close-up images of area in (a) depicted with a solid-line square. These images, with the irregular distribution of the brighter atoms, illustrate the intermixing between Ge and Si atoms. Scanning parameters: (a) 120 nm × 100 nm, 1.8 V, 0.15 nA; (c) 45 nm × 45 nm, 1.2 V, 0.15 nA; (d) 45 nm × 45 nm, −1.2 V, 0.15 nA; (e) 9 nm × 9 nm, −1.0 V, 0.15 nA; (f) 9 nm × 9 nm, −1.5 V, 0.15 nA.

Figure 11(b) is the schematic drawing for the Ge island on (7 × 7) reconstruction. FHUC triangles surrounding the Ge island as a high-energy barrier hinder the further growth in them. Ge will nucleate on the UHUC triangle near the FHUC triangle, as denoted by the black arrow in Figure 11(b), where it has low energy barrier. The energy barrier of FHUC triangle will be reduced by a gain of edge energy, thus the FHUC triangle between the island edge and the UHUC triangle with Ge nucleation will be attached by epitaxy Ge atoms. As a result, the Ge island shows a lateral growth model along its edge, and the shape of Ge islands usually is triangle, which is due to the modulation by the substrate reconstruction.

Figures 11(c) and 11(d) show the island involving in several domains with two different reconstructions, (7 × 7) and (5 × 5). The domain boundaries (defect area) are very clear. Their formation is due to the strains between the substrate and the Ge epitaxy island. The defects on the substrate (like the missing of adatoms and vacancies) will deform the period of (7 × 7) reconstruction and give rise to strain [47, 97]. In addition, the mismatch of the lattice constant of Ge and Si (Ge is 4% larger than Si) will also bring strain. The strains can be effectively released by the formation of the domain boundaries and the different kinds of reconstruction such as the (7 × 7) and (5 × 5) domains shown here.

The (5 × 5) reconstruction also can be described by DAS model [53, 68], as the model shown in Figure 1 for the (7 × 7). Each (5 × 5) unit cell includes one triangle FHUC and one UHUC, and there are three adatoms and one rest atom distributing on the topmost layer in each HUC.

The close-up filled-state STM images in Figures 11(e) and 11(f) show an irregular distribution of brighter adatoms in (7 × 7) unit cell. The arrangement of adatoms, however, is very regular on pure Si(111)-7×7 surface, where the adatoms in the FHUC are imaged brighter than the adatoms in the UHUC, and the corner adatoms are brighter than the center adatoms in both FHUC triangle and UHUC triangle [98]. Here, the brightness and contrast features between adatoms disappear. In Figures 11(e) and 11(f), the corner (or center) adatoms in the same HUC show different brightness, and even some spots at the center adatoms sites are bright close to that of the spots at the corner adatoms sites, so it clearly suggests the mixing condition of Ge and Si atoms. According to the contrast feature of single Ge atoms on Si surface at very low coverage (Figure 5), the brighter protrusions at the center adatoms sites in Figure 11(e) are Ge atoms, and the dimmer ones are Si atoms. These observations are coincided with the findings reported in the earlier literatures [81, 82, 99, 100], where the Ge-Si exchange in Si(111)-5 × 5 Ge reconstructions has been proposed. Most recent results by Voigtländer et al. provided evidences for the exchange and intermixing of Ge/Si in Si(111)-7 × 7 surface at high temperatures by their special techniques [43, 44]. They showed the chemical contrast images between Si and Ge in their STM observations (Ge is much brighter than Si) obtained on Bi-covered Ge/Si(111) surfaces. Thus, the Ge-Si exchanging and intermixing happen at high temperature, and play an important role in the epitaxial growth of Ge islands.

In our high-temperature deposition experiments, when Ge coverage keeps at the range of 0.2 to 0.5 ML, a novel local reconstruction with an ordered arrangement of Ge atoms on the Si(111) surfaces is obtained. Figure 12 shows the STM images of such Ge-induced reconstruction, which coexists with the Si(111)-7 × 7 reconstruction. The local reconstruction emerges not only inside the Ge island (Figure 12(a)) but also inside the original (7 × 7) surface (Figure 12(b)). The triangle domain runs over 30 nm in edge length. The close-up image in Figure 12(c) illustrates the local atomic structure with a hexagonal arrangement. The atomic density is higher than the normal (7 × 7)

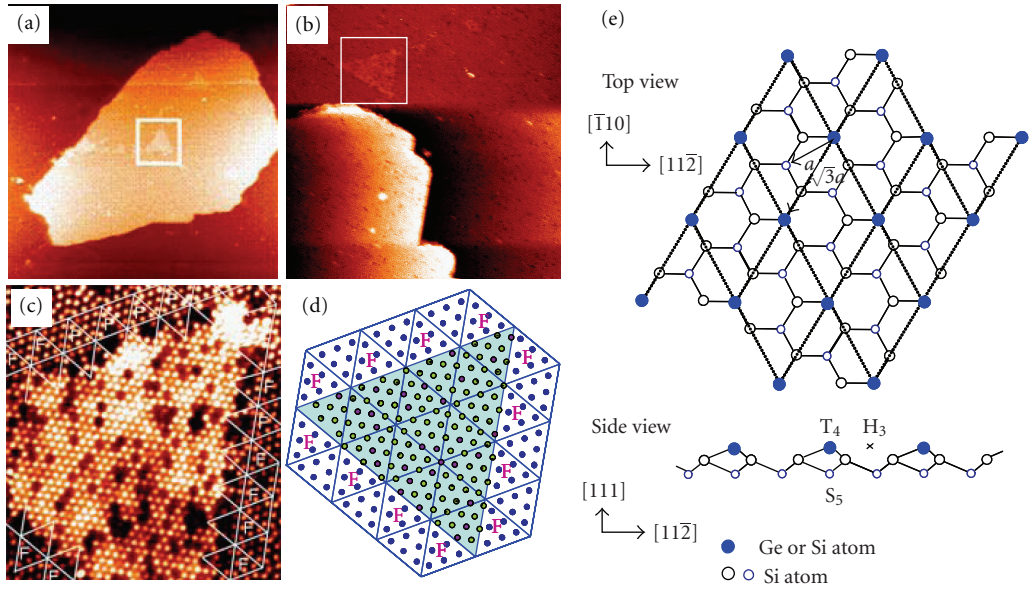

FIGURE 12: STM images of 0.45 ML Ge on the Si(111)-7 × 7 surface. The substrate temperature was held at 300°C for the Ge deposition. Local $(\sqrt{3} \times \sqrt{3})R30^\circ$ reconstruction (marked by the white squares) emerges inside the Ge island in (a) and the Si(111)-7 × 7 substrate in (b). (c) High-resolution image of triangle domain. (d) Schematic of the atomic arrangement of the $(\sqrt{3} \times \sqrt{3})R30^\circ$ domain surrounded by FHUC triangles. (e) Schematic top and side views of the atomic arrangement for the $(\sqrt{3} \times \sqrt{3})R30^\circ$ reconstruction with the adatoms at the T_4 sites. The images are recorded at 2.0 V, 0.10 nA in (a), and 1.4 V, 0.20 nA in (b) and (c). Image sizes: (a) 236 nm × 236 nm, (b) 123 nm × 123 nm, and (c) 22 nm × 24 nm.

reconstruction and the orientation of atom rows is different from the surrounding (7 × 7) lattice alignment. The distance between the neighbor atoms is 0.65 ± 0.01 nm, that is, about $\sqrt{3}$ times the length of the basis vector (0.38 nm) for the ideal bulk-terminated Si(111)-1 × 1 unit cell. In addition, we measured the angle between the main direction of the new local reconstruction and the boundary of the nearby (7 × 7) unit cells and found it to be 30°. Thus, the local reconstruction shows a $(\sqrt{3} \times \sqrt{3})R30^\circ$ arrangement.

The appearance of images in Figures 12(a) and 12(b) demonstrates that Ge-induced $(\sqrt{3} \times \sqrt{3})R30^\circ$ reconstruction replaces some of the (7 × 7) unit cells, and it does not cover the whole surface or the whole island. The local Ge nanostructures thus coexist with the Si(111)-(7 × 7) reconstruction. In addition, several dimmer features at some atom positions exist within the $(\sqrt{3} \times \sqrt{3})R30^\circ$ reconstruction (Figure 12(c)), suggesting that Si atoms are mixed with the Ge atoms.

The schematic in Figure 12(d) shows the atomic arrangement of the $(\sqrt{3} \times \sqrt{3})R30^\circ$ domain surrounded by the FHUC triangles of (7 × 7) unit cells. As the above-mentioned analysis for the similar structure of Ge island boundary in Figure 11(b), removing the reconstruction of the FHUC triangles requires to overcome a larger energy barrier [96]. The activation energy for atom rearrangement in FHUC halves is higher than that in UHUC halves. Thus, the $(\sqrt{3} \times \sqrt{3})R30^\circ$ domain propagates energy preferentially in UHUC triangles.

We further go inside the bonding structure of the local $(\sqrt{3} \times \sqrt{3})R30^\circ$ arrangement with support from the first-principle calculations. When the top-layer atoms form a $(\sqrt{3} \times \sqrt{3})R30^\circ$ reconstruction on Si(111), the underlying substrate changes its original (7 × 7) reconstruction to (1 × 1) arrangement. On an ideal unreconstructed Si(111) surface, there are two types of threefold symmetric adsorption sites, known as T_4, a filled position directly above a second-layer Si atom and H_3, a hollow site above a fourth-layer Si atom sites [88, 90], as shown in Figure 12(e). The adsorbed atoms at either T_4 or H_3 sites are bonded to three first-layer Si atoms. When the dangling bonds of all the first-layer Si atoms are saturated in this way, the adsorbed atoms form a $(\sqrt{3} \times \sqrt{3})R30^\circ$ reconstruction. Such a reconstruction could also be formed when the adsorbed atoms occupy the so-called S_5 site (Figure 12(e)), in which an adsorbed atom substitutes a second-layer Si atom while the replaced Si atom is at the T_4 site directly above S_5 [16, 101, 102]. Our collaborators have performed the first-principle DFT calculations for a $(\sqrt{3} \times \sqrt{3})R30^\circ$ reconstruction. In the case of the Ge-S_5 configuration, Ge or Si forms an adlayer with a Ge coverage of 1/3 monolayer for each of the three bonding configurations [103].

The calculations show that the T_4 configuration is the most stable structure. Its total energy is lower than both the H_3 and the S_5 configurations by 0.60 and 0.68 eV per unit cell, respectively. This is consistent with the general picture that the adatoms prefer to occupy the T_4 sites on almost all of the Si(111)-$(\sqrt{3} \times \sqrt{3})R30^\circ$ surfaces induced by chemisorptions of groups III, IV, and V atoms [101]. The occurrence of Ge atoms in the subsurface substitutional S_5 sites is usually adopted by small atoms such as boron and carbon [104–107], and is energetically unfavorable. Occupation of a Ge atom at the subsurface S_5 site would

introduce significant strain energy due to its larger size than Si. In addition, for the Ge-S_5 configuration, fully filled Ge-associated bands do not warrant a charge transfer from the Si dandling bond to the subsurface to decrease the surface energy as observed in the boron-induced S_5 configuration [108]. Therefore, Ge atoms would prefer to stay on the surface. While the underlying substrate supporting the Ge-induced $(\sqrt{3} \times \sqrt{3})R30^\circ$ structure has an unreconstructed Si(111) configuration, and significant structural relaxation is also found.

3. CONCLUSIONS

Firstly, we reported UHV-STM experiments and first-principle total energy calculations which are combined to determine the STM images of Si(111)-7×7 surface. Both the rest atoms and adatoms were observed simultaneously with high contrast by using the conventional W tips. The emergence of the rest atoms was dependent on the sample bias voltage. The rest atom spots could be visible at the bias voltages less than -0.7 V, and their brightness is even comparable to that of the center Si adatoms when the voltage is less than -0.9 V. The possible explanations for the visibility of rest atoms in our STM images were discussed and a very sharper tip could resolve them, which were enunciated by first-principle calculations.

Secondly, we investigated the structural characterizations and the bonding nature of diverse Ge nanostructures on Si(111)-7×7 surface at different deposition stages. We performed STM measurements of the adsorption site of single Ge atom on the Si(111)-7×7 surfaces for a sequence of submonolayer coverages deposited at 150°C. The observations suggested that individual Ge atoms replaced the so-called Si adatoms rather than being adsorbed directly atop of the Si adatoms. Initially, the replacements were random, but distinct patterns emerged when increasing the Ge coverages, until small clusters are formed on the substrate. The first-principle density-functional calculations revealed that Ge/Si substitution configuration was more energetically favorable and thermodynamically stable than the arrangements of Ge locating at the high-coordination surface sites.

Further deposited Ge atoms generated nanoclusters with varying geometrical configurations. Individual Ge atoms and Ge clusters coexisted on the Si(111)-7×7 surfaces. Ge nanoclusters gradually produced in both the faulted and unfaulted half unit cells of (7×7) units with an initial preference in the faulted halves, and ultimately self-organized into the form of well-ordered hexagonal superlattice corresponding to the geometry of one Ge cluster per triangle half unit of original (7×7) lattice. Charge transfer from Si adatoms to Ge nanoclusters played a key role in the self-organization of the superlattice, which was proved by experimental observations and theoretic calculations.

Two-dimensional extended Ge islands with triangle shape were formed on the substrate when its temperature was kept at 300°C for Ge deposition. The irregular distribution of brighter topmost adatoms suggested the intermixing status of Ge/Si components in the islands, and the intermixing ascribed to the exchanging of Ge atoms with the substrate Si atoms at higher temperatures. Several local domains with different reconstructions like (5×5) and $(\sqrt{3} \times \sqrt{3})R30^\circ$ arrangements were found on the substrates. The configuration of the Ge adatoms residing at the T_4 sites rather than S_5 or H_3 positions in the $(\sqrt{3} \times \sqrt{3})R30^\circ$ reconstruction was proposed according to the first-principle calculations.

ACKNOWLEDGMENTS

The authors are grateful for H. W. Liu, D. X. Shi, and M. C. Xu for experimental assistance, and I. G. Batyrev, W. E. McMahon, S. B. Zhang, A. S. Rao, S. W. Wang, and S. T. Pantelides for theoretic simulations and calculations. This research is supported by the Natural Science Foundation of China (Grants 07JC021N41 and 07JH011N41) and the Chinese National "973" Project.

REFERENCES

[1] G. Binning, H. Rohrer, Ch. Gerber, and E. Weibel, "Surface studies by scanning tunneling microscopy," *Physical Review Letters*, vol. 49, no. 1, pp. 57–61, 1982.

[2] G. Binnig, H. Rohrer, Ch. Gerber, and E. Weibel, "7 × 7 reconstruction on Si(111) resolved in real space," *Physical Review Letters*, vol. 50, no. 2, pp. 120–123, 1983.

[3] Ph. Avouris and R. Wolkow, "Atom-resolved surface chemistry studied by scanning tunneling microscopy and spectroscopy," *Physical Review B*, vol. 39, no. 8, pp. 5091–5100, 1989.

[4] O. Nishikawa, M. Tomitori, F. Iwawaki, and N. Hirano, "Correlation between scanning tunneling microscopy/spectroscopy images and apex profiles of scanning tips," *Journal of Vacuum Science & Technology A*, vol. 8, no. 1, pp. 421–424, 1990.

[5] M. A. Lantz, H. J. Hug, P. J. A. van Schendel, et al., "Low temperature scanning force microscopy of the Si(111)-(7×7) surface," *Physical Review Letters*, vol. 84, no. 12, pp. 2642–2645, 2000.

[6] F. J. Giessibl, S. Hembacher, H. Bielefeldt, and J. Mannhart, "Subatomic features on the silicon (111)-(7 × 7) surface observed by atomic force microscopy," *Science*, vol. 289, no. 5478, pp. 422–425, 2000.

[7] F. J. Giessibl, "Atomic resolution of the silicon (111)-(7 × 7) surface by atomic force microscopy," *Science*, vol. 267, no. 5194, pp. 68–71, 1995.

[8] P. Sutter, P. Zahl, E. Sutter, and J. E. Bernard, "Energy-filtered scanning tunneling microscopy using a semiconductor tip," *Physical Review Letters*, vol. 90, no. 16, Article ID 166101, 4 pages, 2003.

[9] R. J. Hamers, R. M. Tromp, and J. E. Demuth, "Surface electronic structure of Si (111)-(7×7) resolved in real space," *Physical Review Letters*, vol. 56, no. 18, pp. 1972–1975, 1986.

[10] R. S. Becker, B. S. Swartzentruber, J. S. Vickers, and T. Klitsner, "Dimer-adatom-stacking-fault (DAS) and non-DAS (111) semiconductor surfaces: a comparison of Ge(111)-c(2×8) to Si(111)-(2×2), -(5×5), -(7×7), and -(9×9) with scanning tunneling microscopy," *Physical Review B*, vol. 39, no. 3, pp. 1633–1647, 1989.

[11] K. Takayanagi, Y. Tanishiro, M. Takahashi, and S. Takahashi, "Structural analysis of Si(111)-7 × 7 by UHV-transmission

electron diffraction and microscopy," *Journal of Vacuum Science & Technology A*, vol. 3, no. 3, pp. 1502–1506, 1985.

[12] A. Li Bassi, C. S. Casari, D. Cattaneo, et al., "Bulk Cr tips for scanning tunneling microscopy and spin-polarized scanning tunneling microscopy," *Applied Physics Letters*, vol. 91, no. 17, Article ID 173120, 3 pages, 2007.

[13] L. Chen, B. C. Pan, H. Xiang, et al., "Observation of local electronic structures of adatom vacancies in Si (111)-(7 × 7) surface in real space," *Physical Review B*, vol. 75, no. 8, Article ID 085329, 5 pages, 2007.

[14] R. Wiesendanger, *Scanning Probe Microscopy and Spectroscopy: Methods and Applications*, Cambridge University Press, Cambridge, UK, 1994.

[15] S. B. Zhang, M. L. Cohen, and S. G. Louie, "Structural and electronic properties of the Al-GaAs(110) interface," *Physical Review B*, vol. 34, no. 2, pp. 768–772, 1986.

[16] W. Kohn and L. J. Sham, "Self-consistent equations including exchange and correlation effects," *Physical Review*, vol. 140, no. 4A, pp. A1133–A1138, 1965.

[17] G. Kresse and J. Furthmüller, "Efficiency of ab-initio total energy calculations for metals and semiconductors using a plane-wave basis set," *Computational Materials Science*, vol. 6, no. 1, pp. 15–50, 1996.

[18] D. Vanderbilt, "Soft self-consistent pseudopotentials in a generalized eigenvalue formalism," *Physical Review B*, vol. 41, no. 11, pp. 7892–7895, 1990.

[19] J. Tersoff and D. R. Hamann, "Theory of the scanning tunneling microscope," *Physical Review B*, vol. 31, no. 2, pp. 805–813, 1985.

[20] Y.-L. Wang, H.-J. Gao, H.-M. Guo, et al., "Tip size effect on the appearance of a STM image for complex surfaces: theory versus experiment for Si(111)-(7 × 7)," *Physical Review B*, vol. 70, no. 7, Article ID 073312, 4 apges, 2004.

[21] H. Brune, M. Giovannini, K. Bromann, and K. Kern, "Self-organized growth of nanostructure arrays on strain-relief patterns," *Nature*, vol. 394, no. 6692, pp. 451–453, 1998.

[22] I.-S. Hwang, M.-S. Ho, and T. T. Tsong, "Dynamic behavior of Si magic clusters on Si(111) surfaces," *Physical Review Letters*, vol. 83, no. 1, pp. 120–123, 1999.

[23] J.-L. Li, J.-F. Jia, X.-J. Liang, et al., "Spontaneous assembly of perfectly ordered identical-size nanocluster arrays," *Physical Review Letters*, vol. 88, no. 6, Article ID 066101, 4 pages, 2002.

[24] J. Jia, J.-Z. Wang, X. Liu, et al., "Artificial nanocluster crystal: lattice of identical Al clusters," *Applied Physics Letters*, vol. 80, no. 17, pp. 3186–3188, 2002.

[25] J.-F. Jia, X. Liu, J.-Z. Wang, et al., "Fabrication and structural analysis of Al, Ga, and in nanocluster crystals," *Physical Review B*, vol. 66, no. 16, Article ID 165412, 10 pages, 2002.

[26] B. Voigtländer, M. Kästner, and P. Šmilauer, "Magic islands in Si/Si(111) homoepitaxy," *Physical Review Letters*, vol. 81, no. 4, pp. 858–861, 1998.

[27] K. Wu, Y. Fujikawa, T. Nagao, et al., "Na Adsorption on the Si(111)-(7 × 7) surface: from two-dimensional gas to nanocluster array," *Physical Review Letters*, vol. 91, no. 12, Article ID 126101, 4 pages, 2003.

[28] L. Vitali, M. G. Ramsey, and F. P. Netzer, "Nanodot formation on the Si(111)-(7 × 7) surface by adatom trapping," *Physical Review Letters*, vol. 83, no. 2, pp. 316–319, 1999.

[29] H. Hibino and T. Ogino, "Substitution of In for Si adatoms and exchanges between In and Si adatoms on a Si(111)-7 × 7 surface," *Physical Review B*, vol. 55, no. 11, pp. 7018–7022, 1997.

[30] I. Chizhov, G. Lee, and R. F. Willis, "Initial stages of Au adsorption on the Si(111)-(7×7) surface studied by scanning tunneling microscopy," *Physical Review B*, vol. 56, no. 19, pp. 12316–12320, 1997.

[31] Ph. Sonnet, L. Stauffer, and C. Minot, "Adsorption and diffusion mechanisms of Pb on Si(111)-(7 × 7) in the initial stages of Pb chemisorption," *Surface Science*, vol. 407, no. 1–3, pp. 121–132, 1998.

[32] J. M. Gómez-Rodríguez, J. J. Sáenz, A. M. Baró, J.-Y. Veuillen, and R. C. Cinti, "Real-time observation of the dynamics of single Pb atoms on Si(111)-(7 × 7) by scanning tunneling microscopy," *Physical Review Letters*, vol. 76, no. 5, pp. 799–802, 1996.

[33] O. Custance, S. Brochard, I. Brihuega, et al., "Single adatom adsorption and diffusion on Si(111)-(7 × 7) surfaces: scanning tunneling microscopy and first-principles calculations," *Physical Review B*, vol. 67, no. 23, Article ID 235410, 4 pages, 2003.

[34] M. Yoon, X. F. Lin, I. Chizhov, H. A. Mai, and R. F. Willis, "Self-assembled nanodot arrays on Si(111)-(7 × 7) surfaces," *Physical Review B*, vol. 64, no. 8, Article ID 085321, 5 pages, 2001.

[35] X. F. Lin, I. Chizhov, H. A. Mai, and R. F. Willis, "Interaction of Sn atoms with the intrinsic dangling-bond states of Si(111)-(7 × 7)," *Surface Science*, vol. 366, no. 1, pp. 51–59, 1996.

[36] O. Custance, I. Brihuega, J. M. Gómez-Rodríguez, and A. M. Baró, "Initial stages of Sn adsorption on Si(111)-(7 × 7)," *Surface Science*, vol. 482–485, no. 2, pp. 1406–1412, 2001.

[37] Y. P. Zhang, L. Yang, Y. H. Lai, G. Q. Xu, and X. S. Wang, "Formation of ordered two-dimensional nanostructures of Cu on the Si(111)-(7 × 7) surface," *Surface Science*, vol. 531, no. 3, pp. L378–L382, 2003.

[38] H. F. Hsu, L. J. Chen, H. L. Hsiao, and T. W. Pi, "Adsorption and switching behavior of individual Ti atoms on the Si(111)-7 × 7 surface," *Physical Review B*, vol. 68, no. 16, Article ID 165403, 10 pages, 2003.

[39] B. Voigtländer and T. Weber, "Growth processes in Si/Si(111) epitaxy observed by scanning tunneling microscopy during epitaxy," *Physical Review Letters*, vol. 77, no. 18, pp. 3861–3864, 1996.

[40] B. Voigtländer, "Scanning tunneling microscopy studies during semiconductor growth," *Micron*, vol. 30, no. 1, pp. 33–39, 1999.

[41] B. Voigtländer, "Fundamental processes in Si/Si and Ge/Si epitaxy studied by scanning tunneling microscopy during growth," *Surface Science Reports*, vol. 43, no. 5–8, pp. 127–254, 2001.

[42] B. Voigtländer, M. Kawamura, N. Paul, and V. Cherepanov, "Formation of Si/Ge nanostructures at surfaces by self-organization," *Journal of Physics Condensed Matter*, vol. 16, no. 17, pp. S1535–S1551, 2004.

[43] M. Kawamura, N. Paul, V. Cherepanov, and B. Voigtländer, "Nanowires and nanorings at the atomic level," *Physical Review Letters*, vol. 91, no. 9, Article ID 096102, 4 pages, 2003.

[44] N. Paul, S. Filimonov, V. Cherepanov, M. Çakmak, and B. Voigtländer, "Identification of Ge/Si intermixing processes at the Bi/Ge/Si(111) surface," *Physical Review Letters*, vol. 98, no. 16, Article ID 166104, 4 pages, 2007.

[45] T. Sekiguchi, S. Yoshida, K. M. Itoh, J. Mysliveček, and B. Voigtländer, "One-dimensional ordering of Ge nanoclusters along atomically straight steps of Si(111)," *Applied Physics Letters*, vol. 90, no. 1, Article ID 013108, 3 pages, 2007.

[46] Z. A. Ansari, M. Tomitori, and T. Arai, "Evidence of temperature dependence of initial adsorption sites of Ge atoms on Si (111)-7 × 7," *Applied Physics Letters*, vol. 88, no. 17, Article ID 171902, 3 pages, 2006.

[47] M. Suzuki, R. Negishi, and Y. Shigeta, "Strain and electronic structure of Ge nanoislands on Si(111)-7×7 surface," *Physical Review B*, vol. 72, no. 23, Article ID 235325, 5 pages, 2005.

[48] Y. P. Zhang, L. Yan, S. S. Xie, S. J. Pang, and H.-J. Gao, "Self-assembled growth of ordered Ge nanoclusters on the Si(111)-(7 × 7) surface," *Surface Science*, vol. 497, no. 1–3, pp. L60–L64, 2002.

[49] J. Bęben, I.-S. Hwang, T.-C. Chang, and T. T. Tsong, "Model for surfactant-mediated growth of Ge on Pb-covered Si(111) surfaces," *Physical Review B*, vol. 63, no. 3, Article ID 033304, 4 pages, 2001.

[50] K. Wang, C. Zhang, M. M. T. Loy, and X. Xiao, "Time-dependent tunneling spectroscopy for studying surface diffusion confined in nanostructures," *Physical Review Letters*, vol. 94, no. 3, Article ID 036103, 4 pages, 2005.

[51] C. Zhang, G. Chen, K. Wang, et al., "Experimental and theoretical investigation of single Cu, Ag, and Au atoms adsorbed on Si(111)-(7×7)," *Physical Review Letters*, vol. 94, no. 17, Article ID 176104, 4 pages, 2005.

[52] P. M. Petro, A. Lorke, and A. Imamoglu, "Epitaxially selfassembled quantum dots," *Physics Today*, vol. 54, no. 5, pp. 46–52, 2001.

[53] N. Motta, "Self-assembling and ordering of Ge/Si(111) quantum dots: scanning microscopy probe studies," *Journal of Physics Condensed Matter*, vol. 14, no. 35, pp. 8353–8378, 2002.

[54] Y. P. Zhang, L. Yan, S. S. Xie, S. J. Pang, and H.-J. Gao, "Formation of ordered Ge quantum dots on the Si(111)-(7 × 7) surface," *Applied Physics Letters*, vol. 79, no. 20, pp. 3317–3319, 2001.

[55] A. Lobo, S. Gokhale, and S. K. Kulkarni, "Surface morphology and electronic structure of Ge/Si(111)-7 × 7 system," *Applied Surface Science*, vol. 173, no. 3-4, pp. 270–281, 2001.

[56] L. Yan, H. Yang, H.-J. Gao, S. S. Xie, and S. Pang, "Initial adsorption of Ge on Si(111)- (7 × 7) surface at room temperature," *Surface Science*, vol. 498, no. 1-2, pp. 83–88, 2002.

[57] L. Yan, Y. Zhang, H.-J. Gao, S. S. Xie, and S. Pang, "Formation of two dimension Ge cluster superlattice on Si(111)- (7 × 7) surface," *Surface Science*, vol. 506, no. 1-2, pp. L255–L260, 2002.

[58] F. Ratto, F. Rosei, A. Locatelli, et al., "Composition of Ge(Si) islands in the growth of Ge on Si(111)," *Applied Physics Letters*, vol. 84, no. 22, pp. 4526–4528, 2004.

[59] H.-M. Guo, Y.-L. Wang, H. W. Liu, H.-F. Ma, Z.-H. Qin, and H.-J. Gao, "Formation of Ge nanoclusters on Si(111)-7 × 7 surface at high temperature," *Surface Science*, vol. 561, no. 2-3, pp. 227–232, 2004.

[60] Z. A. Ansari, T. Arai, and M. Tomitori, "Hexagonal arrangement of Ge clusters self-organized on a template of half unit cells of Si(111) -7 × 7 observed by scanning tunneling microscopy," *Surface Science*, vol. 574, no. 2-3, pp. L17–L22, 2005.

[61] A. Zhao, X. Zhang, G. Chen, M. M. T. Loy, and X. Xiao, "Initial stages of the adsorption of Ge atoms on the Si (111) - (7 × 7) surface," *Physical Review B*, vol. 74, no. 12, Article ID 125301, 8 pages, 2006.

[62] F. Ratto, A. Locatelli, S. Fontana, et al., "Diffusion dynamics during the nucleation and growth of Ge/Si nanostructures on Si(111)," *Physical Review Letters*, vol. 96, no. 9, Article ID 096103, 4 pages, 2006.

[63] T. P. Pearsall, "Si-Ge alloys and superlattices for optoelectronics," *Materials Science and Engineering B*, vol. 9, no. 1–3, pp. 225–231, 1991.

[64] L. J. Schowalter, "Heteroepitaxy and strain: applications to electronic and optoelectronic materials," *MRS Bulletin*, vol. 21, no. 4, pp. 18–19, 1996.

[65] A. P. Alivisatos, "Semiconductor clusters, nanocrystals, and quantum dots," *Science*, vol. 271, no. 5251, pp. 933–937, 1996.

[66] C. Westphal, "The study of the local atomic structure by means of X-ray photoelectron diffraction," *Surface Science Reports*, vol. 50, no. 1–3, pp. 1–106, 2003.

[67] F. Boscherini, G. Capellini, L. Di Gaspare, F. Rosei, N. Motta, and S. Mobilio, "Ge-Si intermixing in Ge quantum dots on Si(001) and Si(111)," *Applied Physics Letters*, vol. 76, no. 6, pp. 682–684, 2000.

[68] U. Köhler, O. Jusko, G. Pietsch, B. Müller, and M. Henzler, "Strained-layer growth and islanding of germanium on Si(111)-(7 × 7) studied with STM," *Surface Science*, vol. 248, no. 3, pp. 321–331, 1991.

[69] J. R. Patel, J. A. Golovchenko, J. C. Bean, and R. J. Morris, "X-ray-standing-wave interface studies of germanium on Si(111)," *Physical Review B*, vol. 31, no. 10, pp. 6884–6886, 1985.

[70] B. N. Dev, G. Materlik, F. Grey, R. L. Johnson, and M. Clausnitzer, "Geometrical structures of the Ge/Si(111) interface and the Si(111) (7 × 7) surface," *Physical Review Letters*, vol. 57, no. 24, pp. 3058–3061, 1986.

[71] K. Kajiyama, Y. Tanishiro, and K. Takayanagi, "Reconstructions and phase transitions of Ge on the Si(111)-7×7 surface: II. 7×7 and 5×5 structures stabilized by Ge," *Surface Science*, vol. 222, no. 1, pp. 47–63, 1989.

[72] J. A. Carlisle, T. Miller, and T.-C. Chiang, "Ge chemisorption and alloying on the Si(111)-(7 × 7) surface," *Physical Review B*, vol. 49, no. 19, pp. 13600–13606, 1994.

[73] P. Castrucci, R. Gunnella, M. De Crescenzi, M. Sacchi, G. Dufour, and F. Rochet, "Electronic density of empty states of Ge/Si(111) epitaxial layers: theory and experiment," *Physical Review B*, vol. 60, no. 8, pp. 5759–5769, 1999.

[74] G. H. Takaoka, T. Seki, K. Tsumura, and J. Matsuo, "Scanning tunneling microscope observations of Ge deposition on Si(111)-7×7 surfaces irradiated by Xe ions," *Thin Solid Films*, vol. 405, pp. 141–145, 2002.

[75] M. Grodzicki and M. Wagner, "Cluster molecular-orbital calculations on germanium adsorbed on Si(111) surfaces," *Physical Review B*, vol. 40, no. 2, pp. 1110–1120, 1989.

[76] L. Stauffer, S. Van, D. Bolmont, J. J. Koulmann, and C. Minot, "First stages of Ge adsorption on the Si (111)-7 × 7 surface: experimental and theoretical studies," *Surface Science*, vol. 307–309, part 1, pp. 274–279, 1994.

[77] L. Stauffer, P. Sonnet, and C. Minot, "Electronic and atomic structure of Ge/Si(111)-7 × 7 in the initial stages of Ge chemisorption," *Surface Science*, vol. 371, no. 1, pp. 63–78, 1997.

[78] K. Cho and E. Kaxiras, "Diffusion of adsorbate atoms on the reconstructed Si(111) surface," *Surface Science*, vol. 396, no. 1–3, pp. L261–L266, 1998.

[79] S. Y. Tong, H. Huang, C. M. Wei, et al., "Low-energy electron diffraction analysis of the Si(111)-7 × 7 structure," *Journal of Vacuum Science & Technology A*, vol. 6, no. 3, pp. 615–624, 1988.

[80] S. Wang, M. W. Radny, and P. V. Smith, "First-principles electronic structure studies for the cluster modeled Si/Si(111) chemisorption system," *Journal of Chemical Physics*, vol. 114, no. 1, pp. 436–444, 2001.

[81] R. S. Becker, J. A. Golovchenko, and B. S. Swartzentruber, "Tunneling images of the 5×5 surface reconstruction on Ge-Si(111)," *Physical Review B*, vol. 32, no. 12, pp. 8455–8457, 1985.

[82] T. Fukuda, "Random adatom heights in Ge/Si(111)-5×5 surfaces," *Surface Science*, vol. 351, no. 1–3, pp. 103–110, 1996.

[83] F. Rosei, N. Motta, A. Sgarlata, G. Capellini, and F. Boscherini, "Formation of the wetting layer in Ge/Si(111) studied by STM and XAFS," *Thin Solid Films*, vol. 369, no. 1, pp. 29–32, 2000.

[84] J. P. Perdew and Y. Wang, "Accurate and simple analytic representation of the electron-gas correlation energy," *Physical Review B*, vol. 45, no. 23, pp. 13244–13249, 1992.

[85] K. Cho and E. Kaxiras, "Intermittent diffusion on the reconstructed Si(111) surface," *Europhysics Letters*, vol. 39, no. 3, pp. 287–292, 1997.

[86] I.-W. Lyo and Ph. Avouris, "Atomic scale desorption processes induced by the scanning tunneling microscope," *Journal of Chemical Physics*, vol. 93, no. 6, pp. 4479–4480, 1990.

[87] Y.-L. Wang, H.-J. Gao, H.-M. Guo, S. Wang, and S. T. Pantelides, "Bonding configurations and collective patterns of Ge atoms adsorbed on Si(111)-(7×7)," *Physical Review Letters*, vol. 94, no. 10, Article ID 106101, 4 pages, 2005.

[88] J. E. Northrup, "Origin of surface states on Si(111)-(7×7)," *Physical Review Letters*, vol. 57, no. 1, p. 154, 1986.

[89] K. D. Brommer, M. Galvan, A. Dal Pino Jr., and J. D. Joannopoulos, "Theory of adsorption of atoms and molecules on Si(111)-(7×7)," *Surface Science*, vol. 314, no. 1, pp. 57–70, 1994.

[90] M. Y. Lai and Y.-L. Wang, "Self-organized two-dimensional lattice of magic clusters," *Physical Review B*, vol. 64, no. 24, Article ID 241404, 4 pages, 2001.

[91] H. H. Chang, M. Y. Lai, J. H. Wei, C. M. Wei, and Y.-L. Wang, "Structure determination of surface magic clusters," *Physical Review Letters*, vol. 92, no. 6, Article ID 066103, 4 pages, 2004.

[92] M. A. K. Zilani, H. Xu, T. Liu, et al., "Electronic structure of Co-induced magic clusters grown on Si(111)-(7×7) : scanning tunneling microscopy and spectroscopy and real-space multiple-scattering calculations," *Physical Review B*, vol. 73, no. 19, Article ID 195415, 5 pages, 2006.

[93] E. Vasco, C. Polop, and E. Rodríguez-Cañas, "Aggregation mechanisms in the adsorption of metals on Si(111)-7×7," *Physical Review B*, vol. 67, no. 23, Article ID 235412, 10 pages, 2003.

[94] H.-F. Ma, Z.-H. Qin, M. C. Xu, et al., "Formation and evolution of a self-organized hierarchy of Ge nanostructures on Si (111)-(7×7): STM observations and first-principles calculations," *Physical Review B*, vol. 75, no. 16, Article ID 165403, 5 pages, 2007.

[95] M. Suzuki and Y. Shigeta, "Growth of nanoscale Ge magic islands on Si(111)-7×7 substrate," *Surface Science*, vol. 539, no. 1–3, pp. 113–119, 2003.

[96] W. Shimada and H. Tochihara, "Step-structure dependent step-flow: models for the homoepitaxial growth at the atomic steps on Si(111)-7×7," *Surface Science*, vol. 311, no. 1-2, pp. 107–125, 1994.

[97] M. Itoh, H. Tanaka, Y. Watanabe, M. Udagawa, and I. Sumita, "Classification and structure analyses of domain boundaries on Si(111)," *Physical Review B*, vol. 47, no. 4, pp. 2216–2227, 1993.

[98] L. Andersohn, Th. Berke, U. Köhler, and B. Voigtländer, "Nucleation behavior in molecular beam and chemical vapor deposition of silicon on Si(111)-(7×7)," *Journal of Vacuum Science &Technology A*, vol. 14, no. 2, pp. 312–318, 1996.

[99] N. Motta, A. Sgarlata, R. Calarco, et al., "Growth of Ge-Si(111) epitaxial layers: intermixing, strain relaxation and island formation," *Surface Science*, vol. 406, no. 1–3, pp. 254–263, 1998.

[100] P. Martensson, W-X. Ni, G. V. Hansson, J. M. Nicholls, and B. Reihl, "Surface electronic structure of Si(111)7×7-Ge and Si(111)5×5-Ge studied with photoemission and inverse photoemission," *Physical Review B*, vol. 36, no. 11, pp. 5974–5981, 1987.

[101] W. Mönch, *Semiconductor Surfaces and Interfaces*, Springer, New York, NY, USA, 2001.

[102] S. Wang, M. W. Radny, and P. V. Smith, "Ab initio HF/DFT studies of the chemisorption of hydrogen on the cluster simulated Si(111)-$(\sqrt{3}\times\sqrt{3})$R30°-A1 and -Ga surfaces," *Surface Science*, vol. 396, no. 1–3, pp. 40–51, 1998.

[103] Z.-H. Qin, D. X. Shi, H.-F. Ma, et al., "STM observation and first-principles determination of Ge nanoscale structures on Si(111)," *Physical Review B*, vol. 75, no. 8, Article ID 085313, 5 pages, 2007.

[104] P. Castrucci, A. Sgarlata, M. Scarselli, and M. De Crescenzi, "STM study of acetylene reaction with Si(111): observation of a carbon-induced Si(111)-$(\sqrt{3}\times\sqrt{3})$R30° reconstruction," *Surface Science Letters*, vol. 531, no. 1, pp. 329–334, 2003.

[105] X. Peng, L. Ye, and X. Wang, "Carbon induced $(\sqrt{3}\times\sqrt{3})$R30° reconstruction on Si(111) surface: a theoretical study," *Surface Science*, vol. 548, no. 1–3, pp. 51–58, 2004.

[106] C. A. Pignedoli, A. Catellani, P. Castrucci, et al., "Carbon induced restructuring of the Si(111) surface," *Physical Review B*, vol. 69, no. 11, Article ID 113313, 4 pages, 2004.

[107] G. Profeta, L. Ottaviano, and A. Continenza, "$(\sqrt{3}\times\sqrt{3})$R30°$\rightarrow3\times3$ distortion on the C/Si(111) surface," *Physical Review B*, vol. 69, no. 24, Article ID 241307, 4 pages, 2004.

[108] S. Wang, M. W. Radny, and P. V. Smith, "Mechanisms for the stability of Al and B adatoms on the Si(111)-$(\sqrt{3}\times\sqrt{3})$R30° surface," *Physical Review B*, vol. 59, no. 3, pp. 1594–1597, 1999.

Research Letters in Materials Science

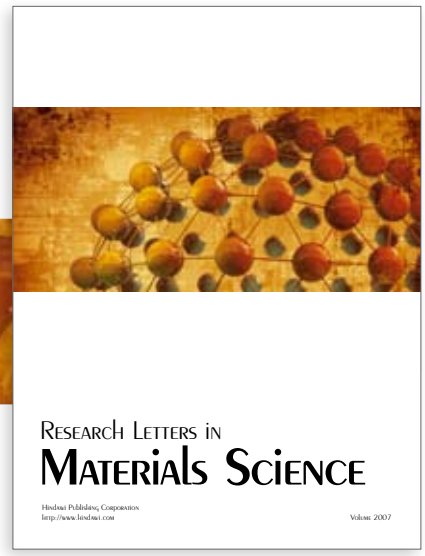

Why publish in this journal?

Research Letters in Materials Science is devoted to very fast publication of short, high-quality manuscripts in the broad field of materials science. Manuscripts should not exceed 4 pages in their final published form. Average time from submission to publication shall be around 60 days.

Why publish in this journal?

Wide Dissemination

All articles published in the journal are freely available online with no subscription or registration barriers. Every interested reader can download, print, read, and cite your article

Quick Publication

The journal employs an online "Manuscript Tracking System" which helps streamline and speed the peer review so all manuscripts receive fast and rigorous peer review. Accepted articles appear online as soon as they are accepted, and shortly after the final published version is released online following a thorough in-house production process.

Professional Publishing Services

The journal provides professional copyediting, typesetting, graphics, editing, and reference validation to all accepted manuscripts.

Keeping Your Copyright

Authors retain the copyright of their manuscript, which are published using the "Creative Commons Attribution License," which permits unrestricted use of all published material provided that it is properly cited.

Extensive Indexing

Articles published in this journal will be indexed in several major indexing databases to ensure the maximum possible visibility of each published article.

Submit your Manuscript Now...

In order to submit your manuscript, please visit the journal's website that can be found at **http://www.hindawi.com/journals/rlms/** and click on the "Manuscript Submission" link in the navigational bar.

Should you need help or have any questions, please drop an email to the journal's editorial office at **rlms@hindawi.com**

ISSN: 1687-6822; e-ISSN: 1687-6830; doi:10.1155/RLMS

Hindawi Publishing Corporation
410 Park Avenue, 15th Floor, #287 pmb, New York, NY 10022, USA
HINDAWI